Bioorg. Med. Chem. 68 (2022) 116807

Contents lists available at ScienceDirect

Bioorganic & Medicinal Chemistry

journal homepage: www.elsevier.com/locate/bmc

Evaluation of chromane derivatives: Promising privileged scaffolds for lead discovery within Alzheimer's disease

Amina Moutayakine [a,b], Carolina Marques [a], Óscar López [c], Donatella Bagetta [d,e], Luisa Leitzbach [f], Stefanie Hagenow [f], Elisabete P. Carreiro [a], Holger Stark [f], Stefano Alcaro [d,e], José G. Fernández-Bolaños [c], Anthony J. Burke [a,g,h,i,*]

[a] LAQV-REQUIMTE, University of Évora, Institute for Research and Advanced Studies, Rua Romão Ramalho, 59, 7000 Évora, Portugal
[b] BioLab, Instituto Universitario de Bio-Orgánica "Antonio González" (IUBO-AG), Centro de Investigaciones Biomédicas de Canarias (CIBICAN), Universidad de La Laguna, Islas Canarias, Spain
[c] Departamento de Química Orgánica, Facultad de Química, Universidad de Sevilla, Apartado 1203, E-41071 Seville, Spain
[d] Dipartimento di Scienze della Salute, Università "Magna Græcia" di Catanzaro, Campus Universitario "S. Venuta", Viale Europa, 88100 Catanzaro, Italy
[e] Net4Science academic spinoff, Università "Magna Græcia" di Catanzaro, Campus Universitario "S. Venuta", Viale Europa, 88100 Catanzaro, Italy
[f] Heinrich Heine University Düsseldorf, Institute of Pharmaceutical and Medicinal Chemistry. Universitaetsstr. 1, 40225 Duesseldorf, Germany
[g] Chemistry Department, School of Science and Technology, University of Évora, Rua Romão Ramalho 59, 7000-671 Évora, Portugal
[h] Faculty of Pharmacy, University of Coimbra, Pólo das Ciências da Saúde, Azinhaga de Santa Comba, 3000-548 Coimbra, Portugal
[i] Coimbra Chemistry Centre, Institute for Molecular Sciences, Faculty of Science and Technology, University of Coimbra, Portugal

A B S T R A C T

The chromane ring system is widely distributed in nature and has proven to be a highly potent pharmacophore in medicinal chemistry, which includes the area of Alzheimer's and Parkinson's diseases. We report on the development of a *gem*-dimethylchroman-4-ol family that was shown to give good inhibition of equine serum butyrylcholinesterase (*eq*BuChE) (in the range 2.9 – 7.3 μM) and in the same range of currently used drugs. We also synthesized a small library of *gem*-dimethylchroman-4-amine compounds, via a simple reductive amination of the corresponding chromanone precursor, that were also selective for *eq*BuChE presenting inhibitions in the range 7.6 – 67 μM. Kinetic studies revealed that they were mixed inhibitors. Insights into their mechanism of action were obtained through molecular docking and STD-NMR experiments, and the most active examples showed excellent drug-likeness and pharmacological properties predicted using Swiss-ADME. We also prepared a set of propargyl *gem*-dimethylchromanamines, for monoamine oxidase (MAO) inhibition but they were only moderately active (the best being 28% inhibition at 1 μM on MAO-B). Overall, our compounds were found to be best suited as inhibitors for BuChE.

1. Introduction

Neurodegenerative diseases such as Parkinson's (PD) and Alzheimer's disease (AD) currently represent a major global health concern; this is exasperated by the exponential increase in elderly individuals at a global level. AD is an age-related multifactorial disorder, characterized by progressive cerebral atrophy leading to cognitive impairment among elderly patients.[1] Some treatments for AD were introduced over the last decades, but unfortunately, they have limited ability to slow down or limit the disease progression and offer no cure (*vide infra*). Consequently, further studies aiming at curing AD remain essential. AD is associated with neuronal damage due to the build-up of β-amyloid (Aβ) plaques outside the neuron leading to neuronal death by disrupting the cell-to-cell communication process, as well as the formation of abnormal hyperphosphorylated tau proteins (neurofibrillary tangles) leading to blockage of nutrient transport into the neurons.[2] Currently, inhibition of acetylcholinesterase (AChE) and butyrylcholinesterase (BuChE) - enzymes involved in the breakdown of acetylcholine (ACh) in the brain - is the standard approach for maintaining the levels of ACh. There are only three FDA approved drugs on the market which act as ChE inhibitors. These include rivastigmine, galantamine and donepezil. Over the last decade many alternatives have been described, some of which are of a hybrid nature, that embrace the Multi-Target-Directed Ligand (MTDL) concept[3], that includes isatin-triazole hybrids and the oxindole-piperidines recently reported by our group.[4–5]

Over recent years, the chromane ring system has gained attention as a privileged scaffold in medicinal chemistry, and particularly as an active agent for the treatment of several neurodegenerative diseases (see the examples in Figure 1). Chromane-based units are ubiquitous in naturally occurring and biologically active compounds. For instance,

* Corresponding author.
E-mail address: ajburke@ff.uc.pt (A.J. Burke).

https://doi.org/10.1016/j.bmc.2022.116807
Received 4 January 2022; Received in revised form 29 April 2022; Accepted 4 May 2022
Available online 9 May 2022

flavonoids which can be categorized as chromane based derivatives are a class of polyphenolic compounds of plant origin having a broad range of pharmacological properties.[6] Among chromane-based structures, chroman-4-ones and chroman-4-ols are particularly interesting as valuable therapeutic candidates, including neurodegenerative disorders.[7] Chromanone scaffolds have been reported to display AChE inhibition activity which occurs through binding with the PAS (peripheral anionic site) of AChE, which was confirmed by several docking studies.[8] For example, a chroman-4-one dithiocarbamate derivative was found to be 4.5-fold more potent than Tacrine, against *ee*AChE (*Electrophorus electricus*) (IC_{50} = 0.10 μM) (Figure 1).[9] In addition, chroman-4-one derivatives were proven to act as a selective inhibitor of Sirtuin-2 associated with age-related neurodegenerative disease.[10] The chromanol ring system has also received considerable attention over the last years as a valuable pharmacophoric scaffold, particularly since the discovery of tocochromanols[11]; these lipid-soluble compounds widely distributed in nature are commonly known as vitamin E. Vitamin E displays significant potency toward oxidative stress implicated in AD by acting as a free radical scavenger (Figure 1).

Monoamine oxidase-B (MAO-B) inhibition has also been a strategy for treating several psychiatric and neurological disorders, including both PD and AD.[12] MAO-B deaminates preferentially β -phenethylamine and benzylamine. In the context of MAO-B inhibition, chromanone derivatives have also shown remarkable inhibitory activity *in vitro*. For example, Wang and coworkers have shown excellent activities against MAO-B (as low as IC_{50} = 8.62 nM, Figure 1) in addition to high selectivities (SI > 11627.9-fold for MAO-B).[13]

Chromane-amines are another valuable target class that exhibit a vast array of pharmacological properties.[14] For instance, chroman-3-amine derivatives were found to possess high affinity for the 5-HT_{1A} receptor,[15] responsible for the prevention of neuronal death, and oxidative stress.[16] Furthermore, the human Bradykinin B1 receptor antagonist which includes a chroman-4-amine unit in its structure,[17] has been linked to the control of neuroinflammation and regulation of amyloid accumulation in AD mice (Figure 1).[18]

As part of our ongoing interest in developing new molecules for targeting Alzheimer's disease, we report our recent results on the chemistry and bioactivity of a new class of diverse chroman-4-one, chroman-4-ols and chroman-4-amine derivatives.

2. Results and discussion

2.1. Chemistry

2.1.1. Gem-Dimethylchroman-4-one and Chroman-4-ol derivatives

Our group reported recently a versatile and useful Pd-catalyzed process to easily access a variety of 3,3-dimethylchroman-4-ols (**2**) and 3,3-dimethylchroman-4-ones (**3**) using a sustainable intramolecular Pd-catalyzed arylation on haloarene-aldehydes (**1**) as starting materials (Scheme 1).[19] The selectivity was controlled by the choice of the ligand and the base, i.e. when bis[(2-diphenylphosphino)phenyl] ether (DPEPhos) and tetrabutylammonium acetate (TBAAc) were used the chroman-2-ol (**2**) is preferred, and when triphenylphosphine (PPh_3) and potassium carbonate (K_2CO_3) were used the chroman-one (**3**) is generally preferred (Scheme 1). Good reaction scope and good yields were observed (with yields up to 97%). Unfortunately, we could only obtain the chroman-4-ol compounds in moderate optical purities on performing asymmetric catalytic reactions, even under optimized conditions. Not only were these compounds of great interest from a medicinal chemistry perspective, particularly in the case of AD, but they all contained a *gem*-dimethyl unit in the pyran ring, which is also of great significance from a medicinal chemistry point of view since this unit is common in various natural products of clinical interest.[20] The *gem*-dimethyl unit generally interacts very positively in the binding pocket of the inhibitors biological target. A good example to demonstrate this point is the case of the blood-pressure controlling drug, Chromakalim[20] (Figure 1) and a group of natural products called the arisugacins, that were isolated from the culture broth of *Penicillum* sp. FO-4259, which were found to exhibit strong AChE inhibition (1 and 25.8 nM, respectively).[21]

To highlight the practicability of this process, we could scale-up the reaction to gram-scale using methyltetrahydrofuran (MeTHF) as a green solvent under the standard conditions affording the intended chromanone (**3a**) in 45% yield (Scheme 2).

2.1.2. Gem-Dimethylchroman-4-amine derivatives

Since our chroman-4-ol compounds were selective BuChE inhibitors with good activities, it was of interest to investigate the activity of their chroman-4-amine analogues. Besides, chiral amines are valuable core units found in various compounds with pronounced pharmaceutical properties. With the purpose of accessing chroman-4-amine derivatives

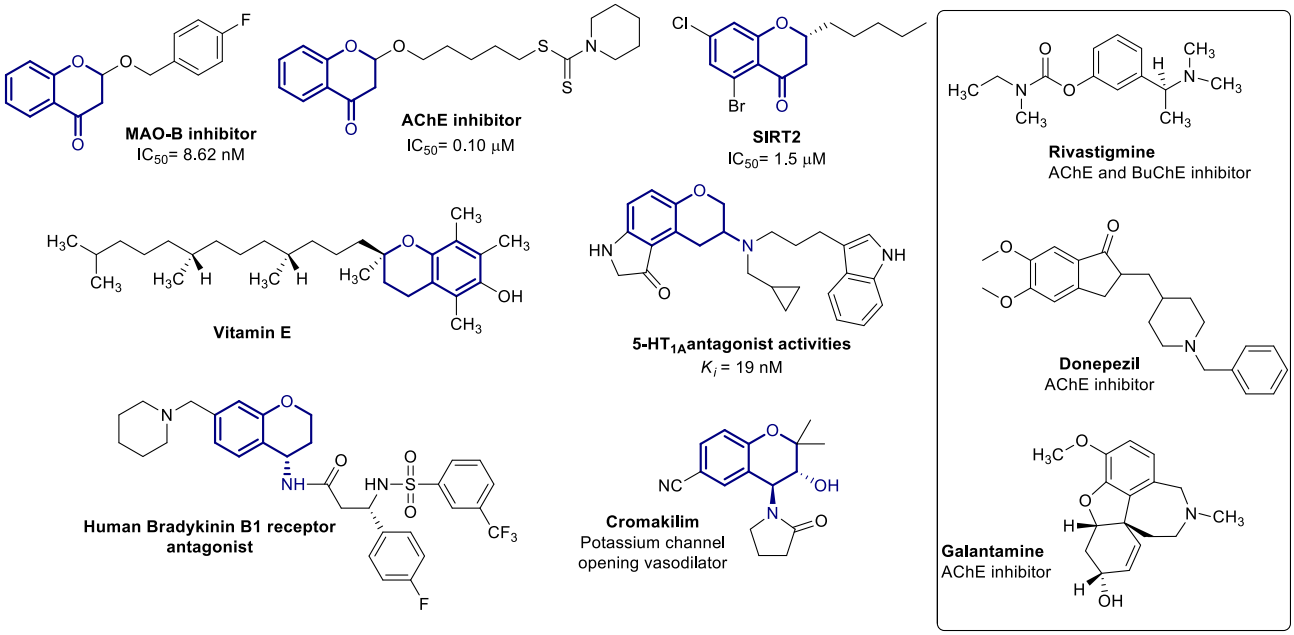

Figure 1. Biologically active chromane-based units and the three clinically available prescribed drugs (rivastigmine, galantamine and donepezil, inset).

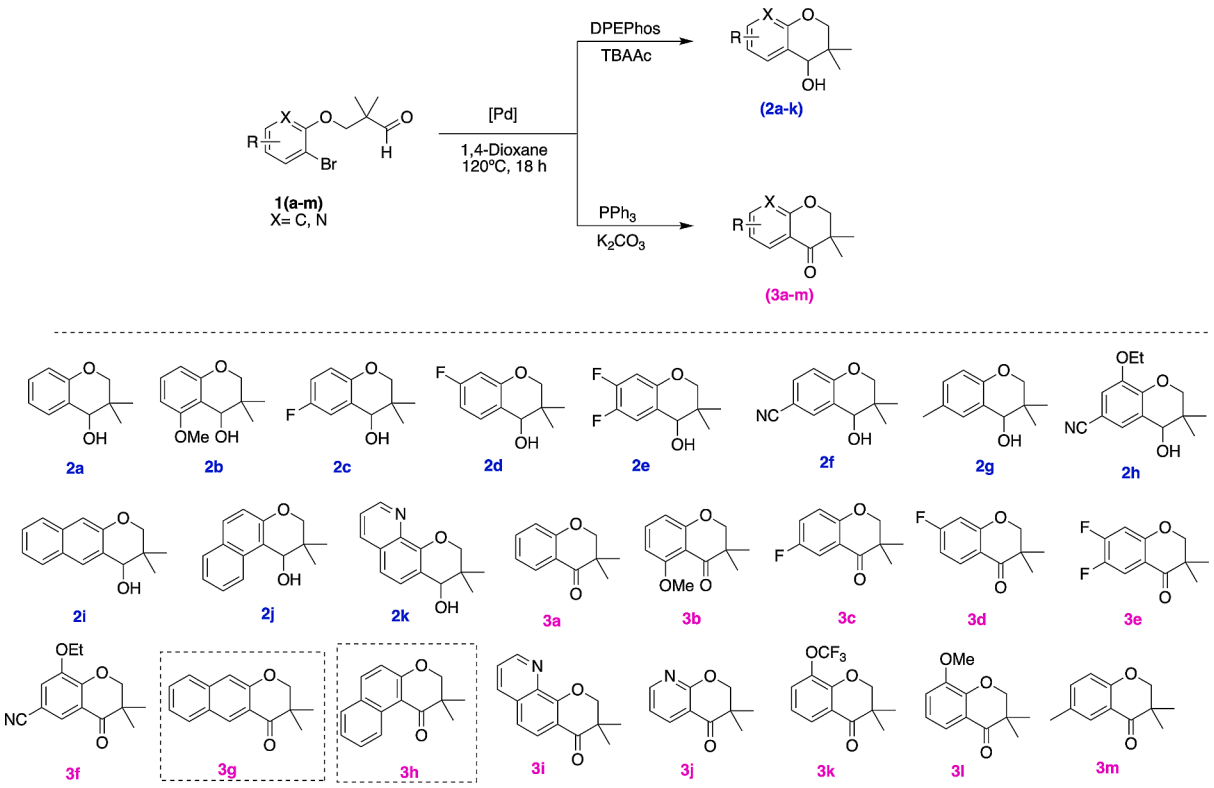

Scheme 1. Pd-Catalyzed intramolecular cyclization of haloarene-aldehyde substrates (**1**) to afford the corresponding 3,3-dimethylchroman-4-ols (**2**) or 3,3 dimethylchroman-4-ones (**3**).

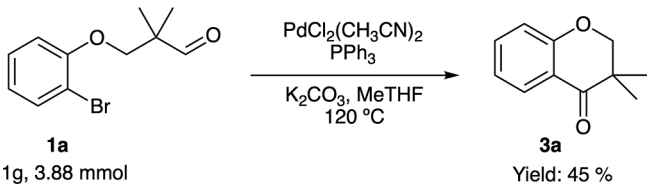

Scheme 2. Gram-scale palladium-catalyzed synthesis of *gem*-2,2-dimethyl-chromanone (**3a**) form (**1a**).

we explored the reductive amination of chroman-4-one substrates. The reductive amination reaction was conducted using a modified Leuckart type reaction that consisted of the use of excess of ammonium acetate (NH_4OAc), aqueous ammonia and sodium cyanoborohydride ($NaBH_3CN$) as reducing agent. The reaction proceeded smoothly under standard conditions affording the desired racemic amines in moderate to good yields (attempts at developing an asymmetric route were unsuccessful) (Scheme 3).

2.1.3. Propargylation and benzylation of gem-Dimethylchroman-4-amine substrates (4)

The propargyl amine "warhead" unit has been used with considerable effect as an effective pharmacophore for inhibiting MAO-B. For instance, both rasagiline, and selegiline, which are selective and covalent MAO-B inhibitors bear a propargyl unit.[12] In our hands, the propargylation of the obtained chromane-4-amine derivatives was carried out under mild conditions using sodium hydride (NaH), propargyl bromide and dimethylformamide (DMF) as solvent (Scheme 4). In the interest of obtaining enantiomerically pure samples, we also examined enantioselective routes to these targets, but all these attempts were unsuccessful. We were also unsuccessful in propargylating compound (**4f**), which gave the corresponding di-propargyl compound (not included in this report). In addition, it should be mentioned that suitable benzylated units have been recognized to be key pharmacophores for MAO inhibition. For instance, 5-benzyloxy and 6-benzyloxyisatin, as well as some benzyloxy phthalimide and benzofuran derivatives (including the flavone analogue given in Figure 1) showed potent *h*MAO-B activities in the low nM range,[12] thwarting us to make the *N*-propargyl-*N*-benzyl derivatives (**5d**) and (**5e**).

3. Biological assays

3.1. Cholinesterase inhibitory activity and SAR analysis

The newly synthesized chromane derivatives were firstly screened for cholinesterase inhibition with *ee*AChE and *eq*BuChE. Galantamine, which is a competitive inhibitor, was used as a positive standard. We observed that this family is selective for BuChE, as all compounds were inactive against AChE. The fact that these compounds were completely selective for BuChE (see Tables 1 and 2), may be a consequence of steric hindrance within the active site cavity originating from the *gem*-dimethyl unit and thus not allowing it to enter fully within the active site

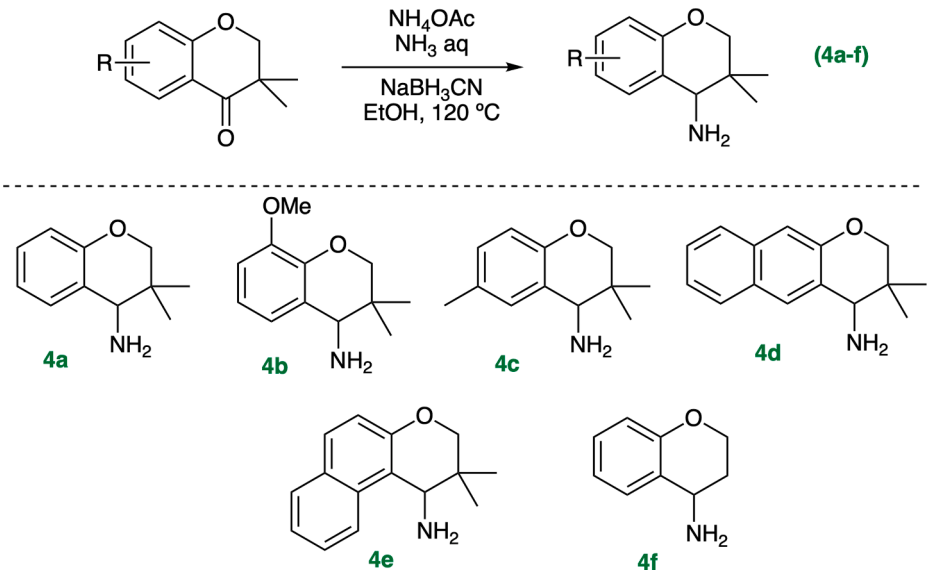

Scheme 3. Preparation of *gem*-dimethylchroman-4-amines (4a)-(**4f**) from (**3l**),(**3g**),(**3h**), (**3a**) and (**3m**) via reductive amination.

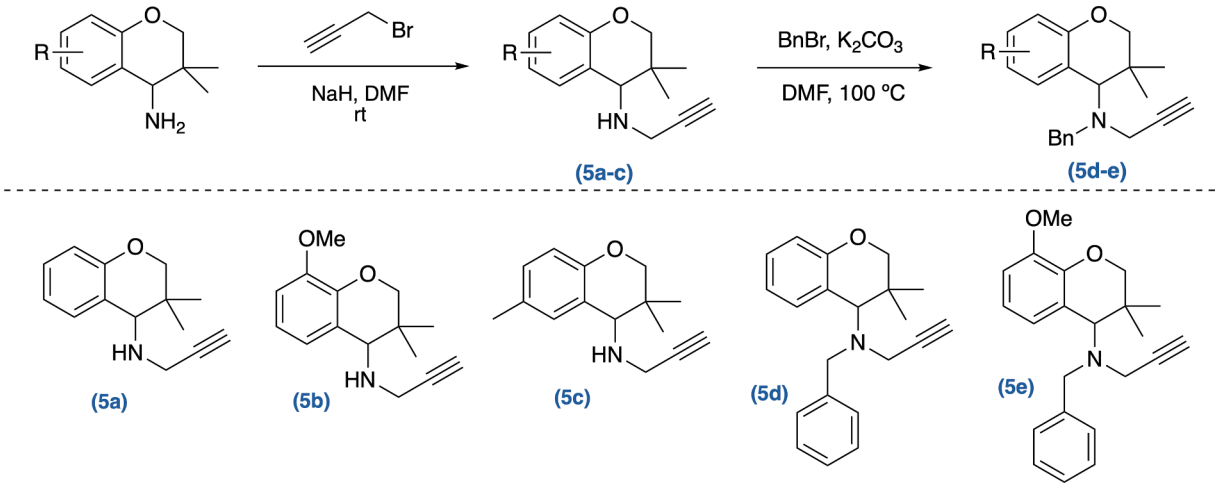

Scheme 4. Propargylation of some *gem*-dimethylchroman-4-amines and subsequent benzylation of *N*-propargyl-*gem*-dimethylchroman-4-amines (**4a**) and (4**b**).

to inhibit the enzyme (being more pronounced in the case of AChE than BuChE), as the active site gorge of the former is much narrower than that of BuChE.[4,5] However, molecular docking studies showed stable interactions between the ligand and such residues as: Tyr341, Tyr124, Trp286 and Phe295 (see Figures s1-s4 Supporting information). The naphthylchromanones (**3g**) and (**3h**) were the most promising compounds, as they displayed the highest potency among the series, with IC_{50} values of 3.1 and 2.9 μM respectively (Table 1), and were slightly more efficient than galantamine, a clinically approved drug for AD. On comparing the naphthylchroman-4-ones with their naphthylchroman-4-ol counterparts (**2i**) and (**2j**), it was found that the latter compounds were 10-fold less potent, exhibiting only moderate inhibitions of 50 μM ((**2i**) and 33 μM (**2j**)), respectively. To further explore the potency of chromane fused compounds, we tested the inhibitory activity of quinoline based chroman-4-one and chroman-4-ols, in this case, both compounds (**2k**) and (**3i**) showed good inhibition against *eq*BuChE with 5.0 μM ((**2k**) and 6.4 μM (**3i**)). Moreover, the potency of the chroman-4-one and chroman-4-ol units was shown to be strongly affected by the substitution pattern and electronic effect of the substituents on the benzene ring. For instance, unsubstituted chroman-4-ol (**2a**) and chroman-4-one (**3a**) exhibited only moderate inhibitory activities of 40 μM ((**2a**)) and 43 μM ((**3a**)) respectively, whereas chroman-4-one (**3k**) with a OCF_3 group at position 8 showed much higher potency (IC_{50} = 4.3 μM). For methoxy-substituted compounds, the position on the aromatic ring had a drastic effect on the inhibition of BuChE, for instance chroman-4-one (**3b**) with a 5-OMe substituent showed a potency of 12 μM, whilst chroman-4-one (**3l**) with a 8-OMe substituent showed no activity. However, chroman-4-ol (**2b**), possessing a 5-OMe group showed no activity. For the fluorinated chroman-4-ols **(2c)** and (**2d**), the presence of a 7-fluoro group gave good activity (18 μM, (**2d**)), whilst incorporation of a 6-fluoro atom (**2c**) gave no activity. The opposite effect was observed amongst the fluorinated chroman-4-ones, the 6-fluorinated chroman-4-one (**3c**) showed moderate potency (33 μM), whilst its 7-fluorinated counterpart (**3d**) was inactive. Chroman-4-ol (**2h**) containing an electron donating ethoxyl group at carbon 8, and an electron withdrawing cyano substituent at carbon 6, was particularly active (7.3 μM) (Table 1).

Both (**2k**) and (**3h**), as model compounds, showed mixed inhibition after conducting kinetic studies using Cornish-Bowden plots, implying that, the inhibitor must be interacting with both, the free enzyme and the enzyme-substrate (E-S) complex (Tables 1 and 2) (see Figure s25-s27; SI).

We also undertook a screening of the chroman-4-amine analogues using similar conditions. Among the tested chroman-4-amine

Table 1
IC_{50} values and inhibition constants for *ee*AChE and *eq*BuChE inhibition with *gem*-dimethylchroman-4-ol (**2**) and *gem*-dimethylchroman-4-one (**3**) derivatives.

Compound	IC_{50} (μM) *ee*AChE[a,b]	IC_{50} and K_i (μM) *eq*BuChE[a,b]
(**2a**)	>100	40 ± 5
(**2b**)	>100	>100
(**2c**)	>100	>100
(**2d**)	>100	18 ± 2
(**2e**)	>100	28 ± 2
(**2f**)	>100	18 ± 1
(**2g**)	>100	>100
(**2h**)	>100	7.3 ± 0.1
(**2i**)	>100	50 ± 5
(**2j**)	>100	33 ± 2
(**2k**)	>100	5.0 ± 0.6 K_{ia} = 7.2 ± 1.9 K_{ib} = 13.7 ± 3.3 Mixed
(**3a**)	>100	43 ± 5
(**3b**)	>100	12 ± 0
(**3c**)	>100	33 ± 4
(**3d**)	>100	>100
(**3e**)	>100	>100
(**3f**)	>100	>100
(**3g**)	>100	3.1 ± 0.2
(**3h**)	>100	2.9 ± 0.3 K_{ia} = 2.0 ± 0.5 K_{ib} = 6.7 ± 1.4 Mixed
(**3i**)	>100	6.4 ± 1.1
(**3j**)	>100	>100
(**3k**)	>100	4.3 ± 0.3
(**3l**)	>100	>100
Galantamine	1.29 ± 0.14	5.47 ± 0.4

[a] Average of 4–6 different inhibitor concentrations and data obtained in duplicate, expressed as the mean ± SD.
[b] At 121 μM substrate concentration for AChE and 112 μM substrate concentration for BuChE.

Table 2
IC_{50} values and kinetic parameters for *eq*BuChE inhibition by *gem*-dimethylchroman-4-amines (**4**).

Compound	IC_{50} (μM) and K_i (μM) eqBuChE[a,b]
(**4a**)	38 ± 9
(**4b**)	7.6 ± 0.6 K_{ia} = 9.0 ± 0.8 K_{ib} = 19.1 ± 0.3
(**4c**)	67 ± 4
(**4d**)	8.9 ± 1.2 K_{ia} = 18 ± 6 μM K_{ib} = 11 ± 2 μM
(**4e**)	52 ± 1

[a] [S] = 112 μM.
[b] A set of 5–6 different inhibitor concentrations was used, and the data were obtained in duplicate and expressed as the mean ± SD.

derivatives, chroman-4-amine (**4b**) with a 8-OMe group provided the highest inhibitory activity against *eq*BuChE (IC_{50} = 7.6 μM). Unsubstituted chroman-4amine (**4a**), and 6-methyl substituted chomane-4-amine (**4e**) showed moderate inhibitory activities of 38 and 52 μM, respectively. Interestingly, the naphthylchroman-4-amine (**4d**) was shown to possess good activity (IC_{50} = 8.9 μM), particularly in comparison with its naphtylchroman-4-amine (**4c**) counterpart that was only moderately active. The kinetic studies showed that both (**4b**) and (**4d**) were mixed inhibitors. Furthermore, compound (**4f**) without a *gem*-dimethyl group was also tested against both AChE and BuChE, it gave an IC_{50} of > 100 μM for the former and only 54% inhibition (at the concentrations refered to in Table 2). This was a clear indication that the *gem*-dimethyl group was important for inhibition in the case of BuChE.

3.2. MAO inhibitory activity

We also examined the MAO activity of these compounds. For this we carried out a selective screening study against both MAO-A and MAO-B. The former catalyzes the oxidative deamination of serotonin (5-HT), adrenaline, noradrenaline, and clorgyline is a selective and irreversible inhibitor[12] whereas dopamine is mainly catabolized by MAO-B having safinamide as reversible inhibitor reference.

3.2.1. MAO inhibition activity of chromanone and chromanols

The MAO inhibition activity of chromane derivatives were conducted at 1 μM, using kynuramine as substrate for MAO-A and B. The highest inhibition activities for MAO-A were obtained with chroman-4-ol (**2a**) and naphthylchroman-4-one (**3h**), showing inhibitions of 24.3% and 23.2%, respectively. The chroman-4-one (**3f**) has also proven to be slightly active against MAO-A, displaying 20.5% inhibition (Table 3). For MAO-B, the highest inhibition activity was obtained with naphthylchroman-4-one (**3g**) (27.7%), and all other compounds showed inhibitions of < 10%. These results were somewhat contrary to the molecular docking studies given below, although the formation of the expected covalent bonds with the FAD cofactor was not factored into these calculations (*vide infra*).

3.2.2. MAO inhibition activity of chroman-4-amines

The selected *gem*-chroman-4-amines showed only low inhibitory activity against both MAO-A and MAO-B (Table 4). In fact, they were marginally more selective against MAO-A than for MAO-B, as the isomeric naphthylchroman-4-amines (**4d**) and (**4e**), gave moderate inhibitions of 13.3% and 12.5%, respectively. Chroman-4-amine (**4d**) also was the best inhibitor of MAO-B (7.5%).

3.2.3. MAO inhibition with N-propargylated chroman-4-amines.

It was also of interest to screen the *N*-propargyl analogues against both MAO-A and B. We expected these analogues to exhibit good MAO inhibition, as they contained the propargyl-amine "warhead"; a residue present in a variety of MAO inhibitors, including rasagiline and has been proposed to establish a covalent bond with the flavin cofactor after putative oxidation by the FAD cofactor within MAO.[22] Those examples containing an 8-OMe unit, namely (**5b**) and (**5e**) demonstrated the best results of 13.8 and 14.7%, respectively, albeit much lower than the positive controls; clorgyline and Safinamide (Table 5). Surprisingly, these values were lower than the best values obtained for their chromane precursors (**2**) and (**3**), which gave values of > 20 % inhibition. However, this might have been due to unfavorable steric hindrance from

Table 3
MAO-A and B screening results for some selected *gem*-dimethylchroman-4-ol (**2**) and *gem*-dimethylchroman-4-one compounds (**3**).

Compound	MAO-A[a] Inhibition [%]	MAO-B[a] Inhibition [%]
(**2a**)	24.3 ± 16.3	8.0 ± 4.1
(**2b**)	11.5 ± 2.3	5.3 ± 2.1
(**2c**)	16.5 ± 3.7	8.3 ± 0.7
(**3a**)	9.7 ± 5.4	9.2 ± 1.7
(**3b**)	12.1 ± 5.6	5.9 ± 2.0
(**3f**)	20.5 ± 18.1	4.7 ± 2.6
(**3g**)	16.4 ± 5.0	27.7 ± 10.9
(**3h**)	23.2 ± 4.3	5.1 ± 4.6
(**3i**)	14.8 ± 1.3	4.8 ± 1.4
Control	0.0 ± 1.9	0.0 ± 0.4
Clorgyline	99.8 ± 0.1	22.6 ± 2.6
Safinamide	9.6 ± 8.9	94.6 ± 1.0

[a] MAO inhibition was calculated as percentages related to control at a test concentration of 1 μM (1 mM stock dissolved in DMSO) and given as mean ± SD of two independent experiments in duplicate.

Table 4
MAO-A and B screening results for some selected *gem*-dimethylchroman-4-amine (**4**) compounds.

Compound	MAO-A[a] inhibition [%]	MAO-B[a] Inhibition [%]
(**4a**)	−3.8 ± 6.7	3.7 ± 2.1
(**4b**)	−0.7 ± 21	4.3 ± 3.7
(**4d**)	13.3 ± 4.5	7.5 ± 1.5
(**4e**)	12.5 ± 6.3	2.7 ± 2.3
(**4f**)	−0.7 ± 14	4.8 ± 2.1
Control	0.0 ± 2.5	0.0 ± 6.6
Clorgyline	100 ± 0.49	23.5 ± 2.8
Safinamide	1.8 ± 2.0	95.7 ± 0.9

[a] MAO inhibition was calculated as percentages related to control at a test concentration of 1 μM (1 mM stock dissolved in DMSO) and given as mean ± SD of two independent experiments in duplicate.

Table 5
MAO-A and B screening results for the *N*-propargyl *gem*-dimethylchroman-4-amine derivatives (**5**).

Compound	MAO-A[a] Inhibition [%]	MAO-B[a] Inhibition [%]
(**5a**)	–	11.6 ± 8.9
(**5b**)	4.6 ± 1.8	13.8 ± 15.5
(**5c**)	−9.4 ± 19[b]	−6.8 ± 22.2
(**5d**)	−10.6 ± 17.2	2.9 ± 3.4
(**5e**)	4.3 ± 1.9	14.7 ± 10.2
Control	−6.0 ± 4.0	0.0 ± 4.0
Clorgyline	100 ± 4.0	24.2 ± 4.0
Safinamide	−0.6 ± 4.0	97.0 ± 1.7

[a] MAO inhibition was calculated as percentages related to control at a test concentration of 1 μM (1 mM stock dissolved in DMSO) and given as mean ± SD of two independent experiments in duplicate. In some cases, the value was negative, this is because the relative fluorescence unit (RFU) values of the inhibitors were higher than those of the control.

the *gem*-dimethyl unit. To address this issue, we attempted to synthesize the non-*gem*-dimethyl *N*-propargyl chroman-4-amine analogues without any success.

In order, to shed light on the possible mechanism of action of our *gem*-dimethylchroman-4-amines with MAO-B we conducted a simple ^{1}H NMR experiment (see section 4). The results of these experiments led us to conjecture that in fact there was no covalent binding between the inhibitor *N*-propargyl unit and the FAD cofactor. In fact, a previous Saturation Transfer Difference (STD)-NMR experiment carried out in our group with this enzyme and commercial rasagaline mesylate, showed no indication of the formation of a covalent bond between the terminal propargyl carbon of the rasagline molecule and the N5 of the FAD cofactor.[23] These studies are continuing in our laboratory in order to obtain further insights.

3.3. Docking studies

3.3.1. With hBuChE

Molecular docking simulations were performed in order to rationalize the interactions of our chromanol and chromanone compounds with human butrylcholinesterase (*h*BuChE). In particular. Table 6 shows the affinity energy of our most promising inhibitors. The binding mode and energy of compound (**3i**) was also computed with the aim to investigate the role of ketone unit in chroman-4-one in comparison to the hydroxyl group in the chroman-4-ol (**2k**). In the case of (**2k**), the molecular docking computations for both enantiomers were carried out. These calculations indicate that (*R*)-(**2k**) should be the best inhibitor in terms of binding affinity energy, but the poses of the two enantiomers in the active site are almost superimposable (Figure 2). Indeed, both ligands perform stacking contacts with the Trp82 by means of their

Table 6
Docking scores (kcal/mol) for binding the *h*BuChE active site.

Compound	Glide Score
(*R*)-(**2k**)	−7.80
(*S*)-(**2k**)	−6.87
(**3g**)	−6.73
(**3h**)	−6.89
(**3i**)	−6.65
X-ray crystal ligand[a]	−8.68

[a] *N*-((1-(2,3-dihydro-1*H*-inden-2-yl)piperidin-3-yl) methyl)-*N*-(2-(dimethylamino)ethyl)-2-naphthamide.

aromatic moieties, meanwhile the hydroxyl group is involved in a hydrogen bond with the catalytic His438 backbone. Moreover compound (**3i**) (Figure 3), lacking the hydroxyl group, was only able to establish stacking contacts with the Phe329 and Trp231 residues. So, the capacity of (**2k**) to form a hydrogen bond with the binding site residue, could explain the better affinity energy of both enantiomers of compound (**2k**) with respect to that of the chroman-4-one derivative (**3i**). Indeed, this was confirmed in the bioassay screen (Table 1, 5μM vs 6.4 μM).

Regarding compounds (**3h**) and (**3g**) it was found that the latter was a weaker binder. In Figure 4, it is possible to observe that both bind to the *h*BuChE binding pocket with a similar configuration characterized by stacking interactions with Trp231 and Phe329. The only difference was the opposite orientation of the chromane moiety. It should be noted that the co-crystallized ligand (as indicated in the footnote to Table 6) in the X-ray crystallography study, and used as reference in our docking studies, gave the best binding energy (-8.68 kcal/mol).

It should be noted that the docking results for some of our compounds against *h*AChE are shown in Table s.1 (supporting information). Compound (**3h**) gave the best binding energy (-8.54 kcal/mol). See also Figure s1-s4 (supporting information) for the enzyme-ligand binding diagram.

3.3.2. With hMAO-B

Prior to the synthesis and the bioassay of compound (**5a**), a molecular docking simulation of both enantiomers was performed suggesting that our *N*-propargylchromane-4-amine derivative could fit into the *h*MAO-B pocket. Indeed, regarding (*R*)-(**5a**) seven poses were obtained and ranked according to the Glide Score (Table 7, Figure 5 and 6 and Figures s5-s20; supporting information).

We observed that the most stable binding modes, endowed with an affinity energy lower than −7 kcal/mol, are superimposable and characterized by stacking interactions with Tyr326 and a hydrogen bond with Ile199. Figure 5 shows the best pose of compound (*R*)-(**5a**) suggested by the docking simulation. Moreover, in the third predicted docking pose (Figure 6) the propargylamine moiety is directed towards the FAD cofactor establishing stacking interactions and a hydrogen bond with Tyr326 and Gln206, respectively. All the other binding modes of compound (*R*)-(**5a**) (Figures s5-s9; supporting information) and compound (*S*)-(**5a**) docking outcomes (Figures s10-s16; supporting information) are shown in the supporting information. Docking outcomes for compound (*S*)-(**5a**) show a similar number of binding modes as for (*R*)-(**5a**) with similar affinity energies (Table s2, supporting information). Also, in one of the suggested binding geometries (Figure s13; supporting information), our compound was calculated to orientate its propargylamine moiety towards the FAD unit and perform stacking interactions with Tyr326 and a hydrogen bond with Leu171. So, for these two enantiomers no relevant differences were observed by molecular docking.

Afterwards, molecular docking simulations of both enantiomers of compounds (**5b**), (**5c**), (**5d**) and (**5e**) were carried out (Table s3, supporting information). According to the results, compounds (**5d**) and (**5e**), endowed with the bulkiest substituents were not able to bind the *h*MAO-B active site. Besides, for the other compounds of this series,

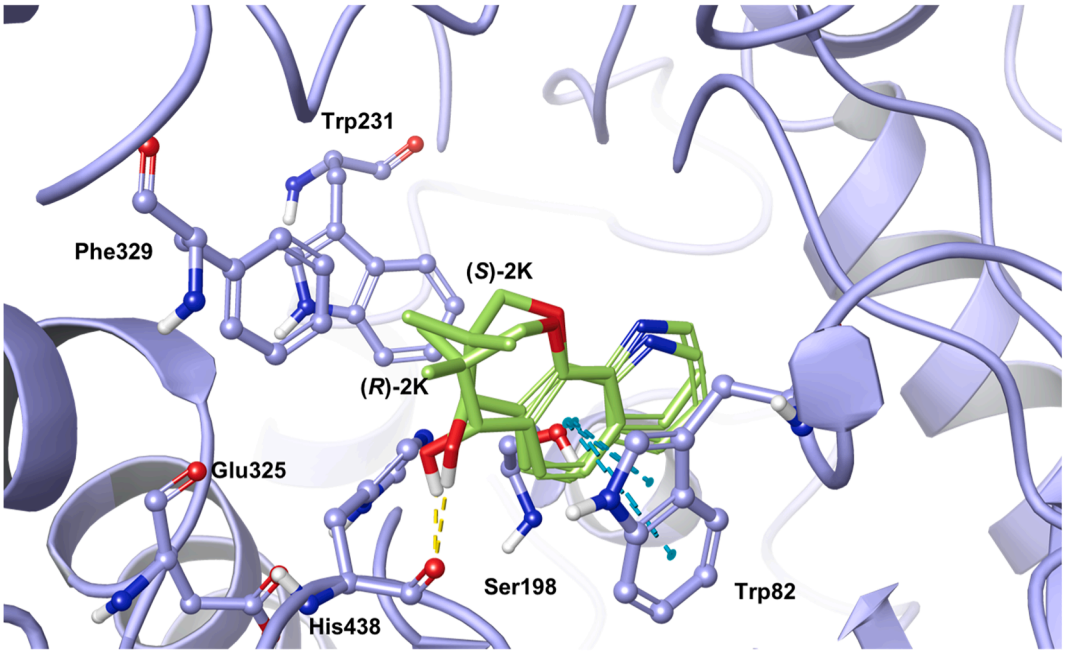

Figure 2. Superimposition of the most stable binding mode of compounds (*R*)-(**2k**) and (*S*)-(**2k**) illustrated in polytube green into the *h*BuChE active site shown as lilac cartoons. Interacting amino acids are depicted in lilac ball and stick representation. Light blue and yellow dotted lines represent π-π interactions and hydrogen bonds respectively.

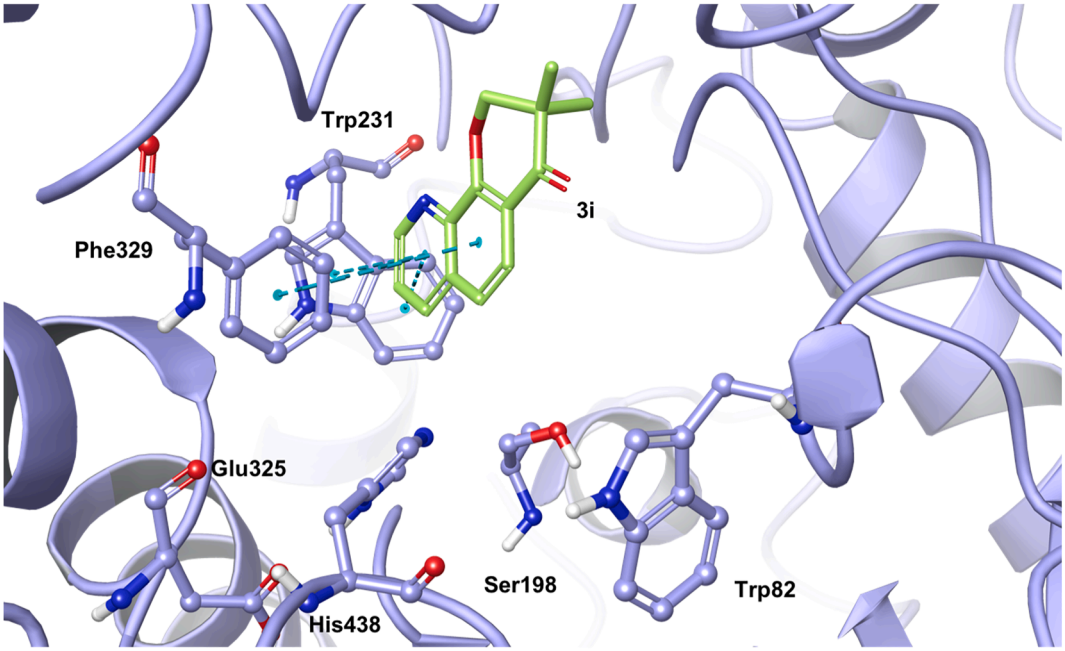

Figure 3. Most stable binding mode of compound (**3i**) illustrated in polytube green into the *h*BuChE active site shown as lilac cartoons. Interacting amino acids are depicted in lilac ball and stick representation. Light blue dotted lines represent π-π interactions.

except for (*R*)-(**5c**), the suggested binding modes were characterized by unfavourable contacts mainly with the Tyr398, Tyr435, Leu171 and Cys172 residues (Figures s17-s20; supporting information). So, these simulations indicate that the recognition of *h*MAO-B by such derivatives of (**5a**) may be hampered by steric hindrance. These types of unfavourable binding contacts were not reported in the binding mode of the X-ray co-crystallized ligand, chlorophenyl-chromone-carboxamide (Figure s21; supporting information) which fitted perfectly into the *h*MAO-B active site establishing a key hydrogen bond interaction with Tyr435 with an affinity energy of −9.86 kcal/mol.

3.4. NMR and saturation Transfer difference (STD)-NMR studies

In order to gain an insight into the interaction of our chromane units with *eq*BuChE, we performed an STD-NMR study on the most potent chromanone (**3h**) and chromane-4- amine (**4b**) units. STD-NMR is a very useful validation technique[24] which we have used previously with success in the past.[25]

3.4.1. STD-NMR of (3h)

On analysis of the ^{1}H NMR spectrum shown in Figure 7 we observed

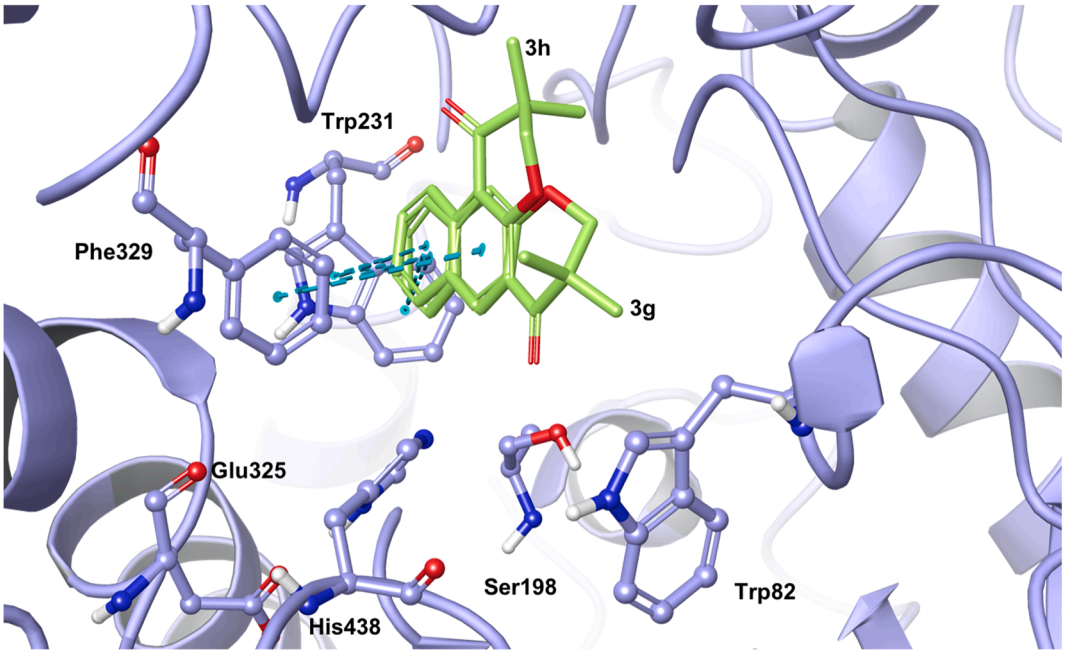

Figure 4. Superimposition of the most stable binding mode of compounds (**3h**) and (**3g**) illustrated in polytube green into the *h*BuChE active site shown as lilac cartoons. Interacting amino acids are depicted in lilac ball and stick representation. Light blue dotted lines represent π-π interactions.

Table 7
Docking scores (kcal/mol) of each pose of compound (*R*)-(**5a**) for binding *h*MAO-B active site.

Pose ranking	Glide Score
1st	−7.58
2nd	−7.54
3rd	−6.67
4th	−6.42
5th	−5.64
6th	−4.84
7th	−4.39

an upfield shift of all the ligand protons indicating extensive magnetic shielding by the *eq*BuChE enzyme. Also, the signals for H5, H4 and H2 overlap which may be due to significant interaction with the enzyme. The graph of the STD amplification factor as a function of saturation time is shown in the supporting information (Figure s22; SI). As can be seen from the epitope intensity map shown in Figure 7, it is the aromatic protons that are affected the most, with attenuations in the range 92–100%. This was in fact supported by the docking study (Figure 4), showing good proximity of the Trp231 (acyl binding pocket) and Phe329 (anionic site) aromatic residues with the inhibitor aromatic protons presumably via π-π interactions. The H-7 methylene protons are the least attenuated protons, indicating weaker interactions with the aromatic enzyme residues.

3.4.2. STD-NMR of (*4b*)

Analysis of the STD epitope map shown in Figure 8 (inset, the most attenuated protons i.e. H2 and H3 were set to 100%) shows that the aromatic H1 and the methoxyl hydrogens are also significantly attenuated, meaning that they are presumably also very close to the enzyme active site residues; Trp231 and Phe329, as are H2 and H3. The methyl group hydrogens (H5; 47% and 39% respectively) have a lower relative STD value indicating that they should be further away from the protein active site residues. Hydrogens H4 and H6, gave almost no STD response indicating that they should be the farthest from the active site surface residues.

3.5. NMR study of (*5a*) with MAO-B

As discussed in section 3.2.1. in an attempt to understand if our *N*-propargylated amine (**5a**) could form a covalent bond with the FAD cofactor, we carried out a decisive NMR study on the interaction of this ligand with the MAO-B enzyme. The ^{1}H NMR experiment was performed by mixing (**5a**) (0.016 mM) in MeOD with MAO-B (0.0084 mM) in 50 mM of potassium phosphate buffer (pH 7.4) in an NMR tube, which was incubated at 37 °C for 20 min. During this incubation time, the ^{1}H NMR spectra were recorded every 5 min, and we observed no significant differences between the different spectra. By comparing the spectrum of inhibitor (**5a**) with the mixture of inhibitor (**5a**) and MAO-B after 20 min (see Fig. s12, SI), we observed some shielding effects on the inhibitor protons, mainly on the propargyl proton, probably due to complexation with the enzyme. However, the existence of the propargyl hydrogen peak in all the recorded spectra was a clear indication that there was no covalent bond formed between the propargyl carbon and the FAD nitrogen.

3.6. Calculated physicochemical properties

Molecular, druglikeness and pharmacokinetic properties were determined for some selected compounds using the SwissADME freeware suite (Table 8).[26]

These simulations revealed that our compounds showed very good properties, and all were compliant with the druglikeness rules of Lipinski, Ghose, Veber, Egan and Muegge, as well as giving zero PAINS (Pan-Assay Interference Compounds) alerts (Table 8). Compounds (**3g**) and (**3h**) showed the best lipophilicities for membrane penetration. Out of interest and for comparative purposes we also conducted the same simulations for our benchmarks, namely, galantamine, clorgyline and safinamide (Table 8). Compounds **(2k)** and **(4b)** showed good total surface area values, comparable to galantamine, indicating good binding to aromatic and hydrophobic units in the enzyme active site. As blood–brain-barrier (BBB) penetration is a crucial issue, gratifyingly our simulations showed that all the selected compounds showed good BBB penetration. They were also predicted to have high gastro-intestinal (GI) permeation.

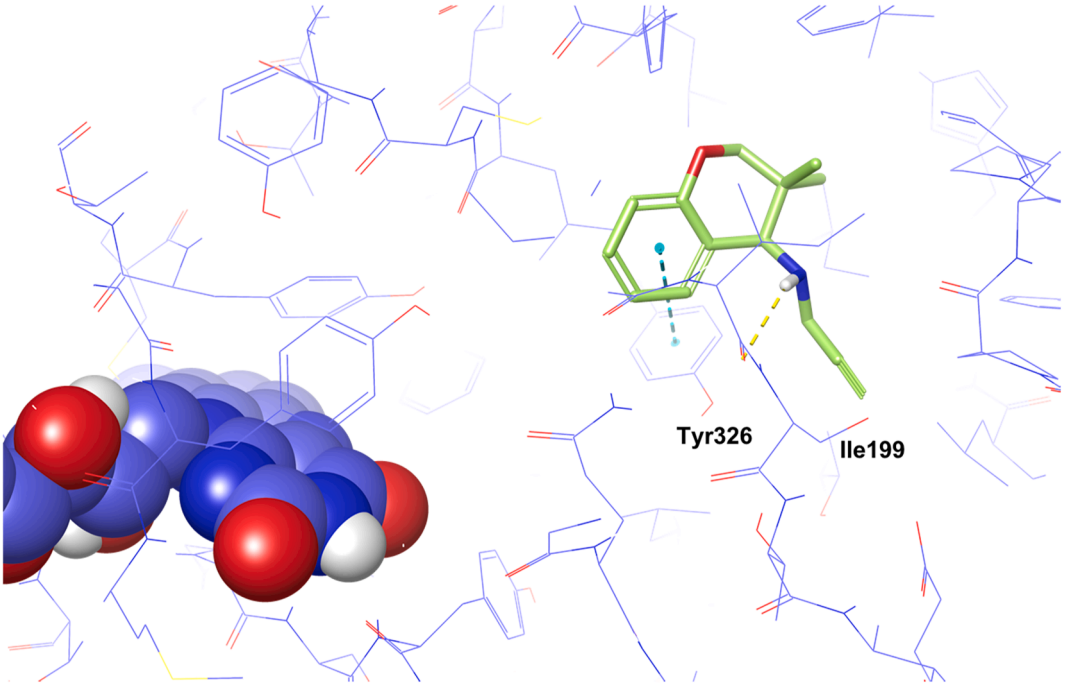

Figure 5. Most stable binding mode of (*R*)-**(5a)** derivative into *h*MAO-B active site shown in purple. The ligand and interacting amino acids are illustrated in green polytubes and purple thin tubes; FAD cofactor is displayed in purple spacefill. Light blue and yellow dotted lines respectively indicate stacking interactions and hydrogen bonds.

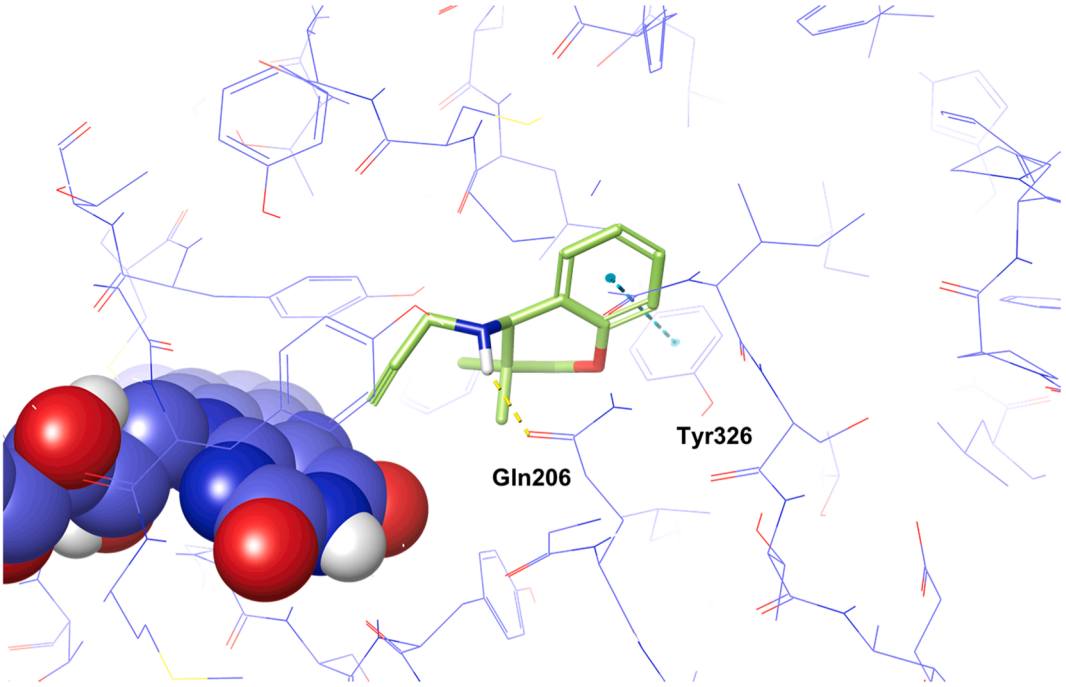

Figure 6. 3rd stable binding mode of (*R*)-(**5a**) derivative into *h*MAO-B active site shown in purple. The ligand and interacting amino acids are illustrated in green polytubes and purple thin tubes; FAD cofactor is displayed in purple space-fill. Light blue and yellow dotted lines respectively indicate stacking interactions and hydrogen bonds.

4. Conclusions

In this study, we screened several chromane-based compounds against *ee*AChE and *eq*BuChE (the common models currently used to determine ChE inhibition). Compounds (**2k**) (chromanol), (**3g**) (chromanone) and (**3h**) (chromanone), showed moderate activity against *eq*BuChE. All our chromane compounds showed no inhibition of *ee*AChE. Compounds (**2a**) and (**3g**) showed moderate activity against MAO-A and MAO-B, with inhibitions of > 20 %, and surprisingly were more active than those obtained for the *N*-propargylated derivatives (**5**). Steric hindrance due to the presence of the 3-*gem*-dimethyl unit was considered the reason for the moderate to low activity of these propargylated amines. In fact, a ^{1}H NMR study of (**5a**) with MAO-B failed to reveal the formation of a covalent bond between the propargyl terminal

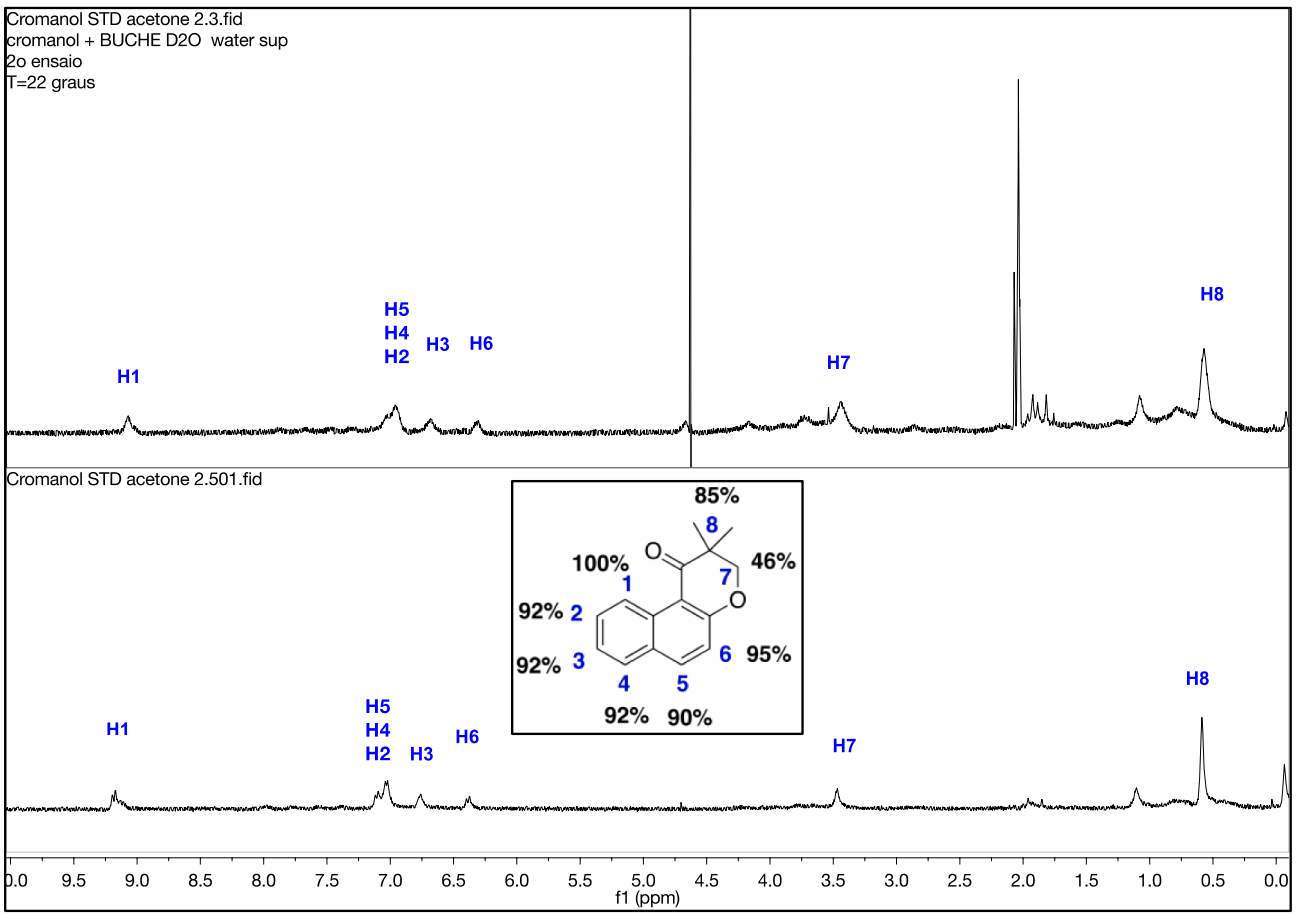

Figure 7. (top) ^{1}H NMR spectrum of *eq*BuChE (4.2 μM) with (**3h**) (1.47 mM) (x 350). (bottom) STD-NMR spectrum at 3 s of saturation time. H1 was set to 100%. The NMR spectra were recorded at 22 °C. The inset shows the epitope intensities derived from the initial STD build-up rates (see SI) and normalized to the largest value (an arbitrary numbering system has been used).

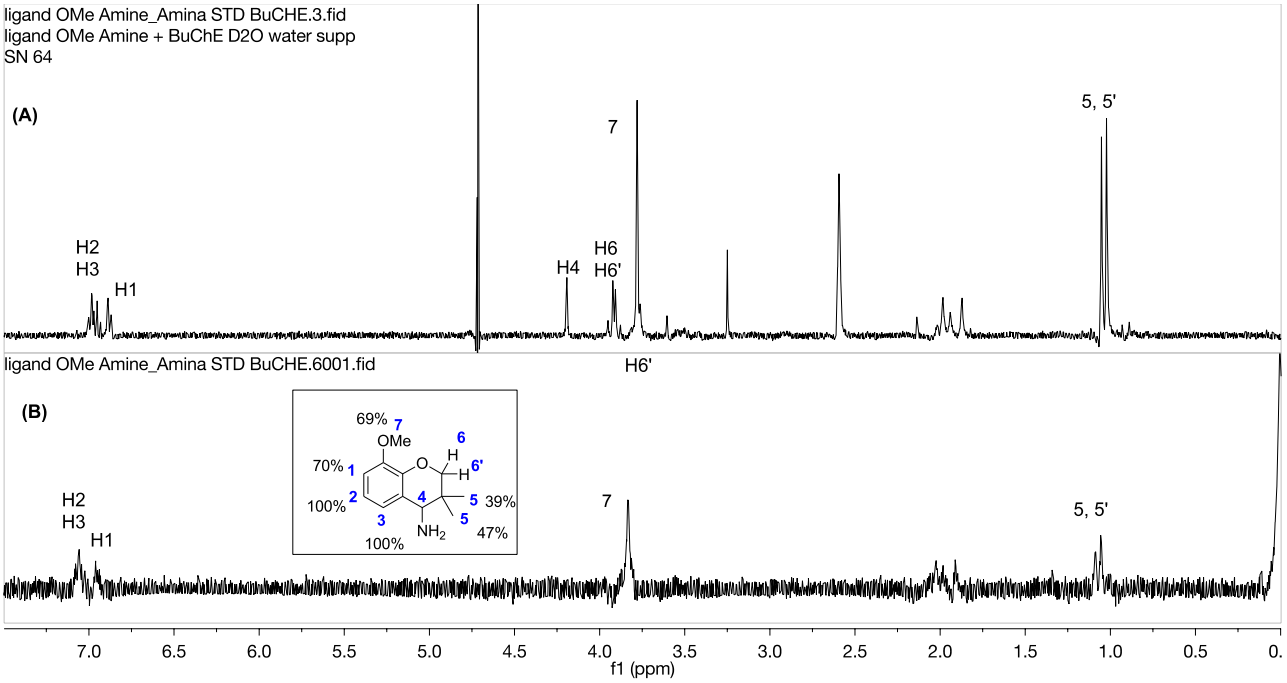

Figure 8. (top) ^{1}H NMR spectrum of *eq*BuChE (4.0 μM) with (**4b**) (0.8 mM) (x 200). (bottom) STD-NMR spectrum at 4 s of saturation time. H2 and H3 were set to 100%. The NMR spectra were recorded at 20 °C. The inset shows the epitope intensities derived from the initial STD build-up rates (see Fig. s23; SI) and normalized to the largest value (an arbitrary numbering system has been used.).

Table 8
Molecular properties for selected compounds (from SwissADME).

Compound	MW (g/mol)	MLOGP[27]	LogS[28]	#H-bond acceptors	#H-bond donors	TPSA	PAINS #alerts
(**2k**)	229.27	1.72	−2.8	3	1	42.35	0
(**3g**)	226.27	2.30	−3.8	2	0	26.30	0
(**3h**)	226.27	2.30	−3.8	2	0	26.30	0
(**4b**)	207.27	1.40	−2.27	3	1	44.48	0
Galantamine	287.35	1.74	−2.34	4	1	41.93	0
Clorgyline	272.17	3.64	−4.15	2	0	12.47	0
Safinamide	302.34	2.41	−3.19	4	2	64.35	0

MW = molecular weight; #H-bond = number of hydrogen bonds; TPSA = topological polar surface area (Å^2).

carbon and N5 of the FAD cofactor, but these studies are still ongoing in our group. Molecular docking and STD-NMR studies indicated the mode of action of these inhibitors within the enzyme active site. With regard to druglikeness, our most active compounds were compliant with the Lipinski, Ghose and other druglikeness compliance rules, and showed good, simulated lipophilicities, as well as BBB and GI penetration. We are currently investigating methods (including biocatalytic means) for accessing chroman-4-amines and derivatives, as well as hybridizing these entities with other key pharmacophores.

5. Experimental

5.1. Synthesis

General considerations: Reagents were obtained from Sigma Aldrich, Acros, Strem and Alfa Aesar and were used as received. The solvents used were dried using standard laboratory techniques. Reactions with transition metal catalysts were conducted in a Radley's 12-position carousel reactor under a nitrogen atmosphere or in round-bottom flasks. Column chromatography was carried out on silica gel (Carlo Erba, 40–63 μm (flash) and 60–200 μm, 60A). Thin-layer chromatography (TLC) was carried out on aluminum-backed Kieselgel 60 $_{F254}$ plates (Merck and Machery Nagel).

Plates were visualized either by UV light or with phosphomolybdic acid in ethanol. NMR spectra were recorded with a Bruker Avance III instrument (400 MHz) with a broad band probe. Chemical shifts are quoted in parts per million (ppm) relative to δ = 0.0 ppm and were referenced to the appropriate non-deuterated solvent peak. Coupling constants (J) are reported in Hz and refer to apparent peak multiplicities. Splitting patterns are reported as s, singlet; d, doublet; t, triplet; m, multiplet; br, broad.

Low-resolution mass spectra (LRMS) were recorded with a quadrupole mass spectrometer Waters ZQ4000 and high-resolution mass spectra (HRMS) on a Thermo Orbitrap Q-exactive focus at a resolution of 70,000 at the Chemistry Department, University of Salamanca (by Dr. César Raposo). ESI was used as ionization method, and the samples were dissolved in methanol. In the case of the HRMS, an alternating method between positive and negative modes was applied and the mode with best signal was used for the determination of the exact mass.

5.1.1. General Procedure for the preparation of the aldehydes

To a round-bottom flask, under a nitrogen atmosphere, was added the following: bromoaryl alcohol ether substrate (3.9 mmol), pyridinium chlorochromate (PCC) (2 equivalents), celite (twice the mass of the PCC used) and freshly distilled DCM (10 mL). The reaction was left stirring overnight at room temperature. The solvent was evaporated under reduced pressure and 20 mL of hexane/AcOEt (5/1) was added to the flask. The mixture was filtered using a sintered glass filter with a layer of celite and a layer of silica gel and washed with 50 mL of hexane/AcOEt (1/1). The solvents were evaporated under reduced pressure to furnish the desired product without further purification.

3-(2-Bromophenoxy)-2,2-dimethylpropanal (1a)[19] Orange oil (81% yield). ^{1}H NMR ($CDCl_3$, 400 MHz) δ: 1.27 (s, CH_3, 6H), 4.00 (s, CH_2, 2H), 6.82–6.90 (m, Ar, 2H), 7.23–7.27 (t, *J* = 8 Hz, Ar, 1H), 7.51–7.53 (d, *J* = 8 Hz, Ar, 1H), 9.71 (s, CHO, 1H). ^{13}C NMR ($CDCl_3$, 100 MHz) δ: 19.3, 74.0, 73.6, 112.5, 113.3, 122.3, 128.5, 133.4, 155.0, 204.5.

3-(2-Bromo-3-methoxyphenoxy)-2,2-dimethylpropanal (1b)[19]: Pale orange oil (57% yield). ^{1}H NMR ($CDCl_3$, 400 MHz) δ: 1.26 (s, CH_3, 6H), 3.88 (s, OCH_3, 3H), 4.00 (s, CH_2, 2H), 6.54–6.58 (t, *J* = 8 Hz, Ar, 2H), 7.18–7.22 (t, *J* = 8 Hz, Ar, 1H), 9.71 (s, CHO, 1H). ^{13}C NMR ($CDCl_3$, 100 MHz) δ: 19.3, 47.0, 56.5, 73.8, 101.7, 105.1, 105.8, 128.33, 156.34, 157.35, 204.6.

3-(2-Bromo-4-fluorophenoxy)-2,2-dimethylpropanal (1c)[19]: Pale yellow oil (87% yield). ^{1}H NMR ($CDCl_3$, 400 MHz) δ: 1.26 (s, CH_3, 6H), 3.96 (s, CH_2, 2H), 6.82–6.85 (m, Ar, 1H), 6.94–6.99 (m, Ar, 1H), 7.27–7.29 (m, Ar, 1H), 9.69 (s, CHO, 1H). ^{13}C NMR ($CDCl_3$, 100 MHz) δ: 19.3, 47.0, 74.3, 112.6–112.7, 113.9–114.0, 114.6–114.9, 120.44–120.7, 151.76–151.79, 155.78–158.2, 204.4.

3-(2-Bromo-5-fluorophenoxy)-2,2-dimethylpropanal (1d)[19]: Pale yellow oil (62% yield). ^{1}H NMR ($CDCl_3$, 400 MHz) δ: 1.27 (s, CH_3, 6H), 3.97 (s, CH_2, 2H), 6.56–6.65 (m, Ar, 2H), 7.42–7.46 (m, Ar, 1H), 9.67 (s, CHO, 1H). ^{13}C NMR ($CDCl_3$, 100 MHz) **δ**: 19.3, 46.8, 73.6, 101.3–101.6, 106.62–106.66, 108.8–109.0, 133.5–133.6, 155.8–155.9, 161.4–163.9, 204.1.

3-(2-Bromo-4,5-difluorophenoxy)-2,2-dimethylpropanal (1e)[19]: Pale yellow oil (84% yield). ^{1}H NMR ($CDCl_3$, 400 MHz) δ: 1.26 (s, CH_3, 6H), 3.94 (s, CH_2, 2H), 6.73–6.78 (m, Ar, 1H), 7.34–7.38 (t, *J* = 8 Hz, Ar, 1H), 9.66 (s, CHO, 1H). ^{13}C NMR ($CDCl_3$, 100 MHz) δ: 19.3, 46.9, 74.3, 102.8–103.0, 105.7–105.8, 121.4–121.6, 143.4–146.0, 148.3–151.6, 150.7–150.9, 203.9.

3-Bromo-4-(2,2-dimethyl-3-oxopropoxy)benzonitrile (1f)[19]: Colourless oil (82% yield). ^{1}H NMR ($CDCl_3$, 400 MHz) δ: 1.28 (s, CH_3, 6H), 4.06 (s, CH_2, 2H), 6.92–6.94 (d, *J* = 8 Hz, Ar, 1H), 7.56–7.59 (m, Ar, 1H), 7.79–7.80 (d, *J* = 4 Hz, Ar, 1H), 9.64 (s, CHO, 1H). ^{13}C NMR ($CDCl_3$, 100 MHz) δ: 19.3, 46.8, 73.4, 106.6, 112.8, 112.9, 117.7, 133.1, 136.7, 158.5, 203.6.

3-(2-Bromo-4-methylphenoxy)-2,2-dimethylpropanal (1g)[19]: Pale yellow oil (73% yield). ^{1}H NMR ($CDCl_3$, 400 MHz) δ: 1.28 (s, CH_3, 6H), 2.29 (s, CH_3, 3H), 3.99 (s, CH_2, 2H), 6.79–6.81 (d, *J* = 8 Hz, Ar, 1H), 7.05–7.07 (d, *J* = 8 Hz, Ar, 1H), 7.36–7.37 (m, Ar, 1H), 9.73 (s, CHO, 1H). ^{13}C NMR ($CDCl_3$, 100 MHz) δ: 19.3, 20.3, 47.0, 73.9, 112.2, 113.4, 128.9, 132.1, 133.8, 153.0, 204.7.

3-Bromo-4-(2,2-dimethyl-3-oxopropoxy)-5-ethoxybenzo nitrile (1i)[19]: Pale yellow oil (54% yield). ^{1}H NMR ($CDCl_3$, 400 MHz) δ: 1.23 (s, CH_3, 6H), 1.45–1.49 (t, *J* = 8 Hz, CH_3,3H), 4.03–4.08 (m, CH_2, 4H), 7.06 (s, Ar, 1H), 7.42 (s, Ar, 1H), 9.75 (s, CHO, 1H). ^{13}C NMR ($CDCl_3$, 100 MHz) δ: 14.6, 19.0, 47.4, 63.3, 77.1, 108.7, 115.6, 117.6, 118.2, 128.9, 149.3, 153.0, 204.5.

3-((1-Bromonaphthalen-2-yl)oxy)-2,2-dimethylpropanal (1j)[19]: Pale yellow oil (78% yield). ^{1}H NMR ($CDCl_3$, 400 MHz) δ: 1.32 (s, CH_3, 6H), 4.15 (s, CH_2, 2H), 7.23–7.25 (d, *J* = 8 Hz, Ar, 1H), 7.39–7.43 (t, *J* = 8 Hz, Ar, 1H), 7.55–7.59 (t, *J* = 8 Hz, Ar, 1H), 7.77–7.81 (t, *J* = 8 Hz, Ar, 2H), 8.20–8.22 (d, *J* = 8 Hz, Ar, 1H), 9.78 (s, CHO, 1H). ^{13}C NMR ($CDCl_3$, 100 MHz) δ: 19.4, 47.2, 74.8, 109.9, 115.1, 124.7, 126.3, 127.9, 128.1, 129.0, 130.2, 133.2, 153.0, 204.6.

3-((7-Bromoquinolin-8-yl)oxy)-2,2-dimethylpropanal (1k)[19]: Brownish oil (41% yield). ^{1}H NMR ($CDCl_3$, 400 MHz) δ: 1.32 (s, CH_3,

6H), 4.48 (s, CH_2, 2H), 7.39–7.44 (m, Ar, 2H), 7.62–7.65 (m, Ar, 1H), 8.10–8.12 (d, J = 8 Hz, Ar, 1H), 8.88–8.90 (m, Ar, 1H), 10.02 (s, CHO, 1H). ^{13}C NMR ($CDCl_3$, 100 MHz) δ: 19.1, 47.7, 78.9, 116.4, 121.5, 124.1, 129.1, 130.8, 136.2, 143.2, 150.0, 152.2, 205.8.

3-(2-Bromo-6-methoxyphenoxy)-2,2-dimethylpropanal (1l)[19]**:** pale yellow oil (82% yield). ^{1}H NMR ($CDCl_3$, 400 MHz) δ: 1.23 (s, CH_3, 6H), 3.83 (s, CH_3, 3H), 4.00 (s, CH, 1H), 6.83–6.85 (d, J = 8 Hz, Ar, 1H), 6.90–6.94 (t, J = 8 Hz, Ar, 1H), 7.10–7.12 (d, J = 8 Hz, Ar, 1H), 9.82 (s, CHO, 1H). ^{13}C NMR ($CDCl_3$, 100 MHz) δ:18.9, 29.7, 47.3, 56.1, 111.7, 117.7, 124.8, 125.2, 145.0, 153.7, 205.3.

3-(2-Bromo-6-(trifluoromethoxy) phenoxy)-2,2-dimethylpropanal (1m)[19]**:** pale yellow oil (75% yield).^{1}H NMR ($CDCl_3$, 400 MHz) δ: 1.31 (s, CH_3, 6H), 4.02 (s, CH_2, 2H), 6.77–6.78 (d, J = 4 Hz, Ar, 2H), 7.54–7.56 (d, J = 12 Hz, Ar, 1H), 9.71 (s, CHO, 1H). ^{13}C NMR ($CDCl_3$, 100 MHz) δ: 19.2, 46.8, 73.5, 106.5, 110.2, 114.3, 119.0, 121.5, 133.6, 149.0, 155.7, 203.8.

5.1.2. General Procedure for the preparation of chromanols and chromanones derivatives

To a Radley's® 12 position carousel reactor tube was added $PdCl_2(CH_3CN)_2$ (10 mol%), the ligand (25 mol%), the corresponding bromoaryl aldehyde substrate (100 mg), the base (3 equivalents) and 1,4-dioxane (2 mL). The reaction was left stirring at 120 °C for 18 h under a nitrogen atmosphere. The solvent was evaporated under reduced pressure and the crude product was purified by silica gel chromatography using Hexane/AcOEt (9/1) as eluent, affording the desired products.

3,3-Dimethylchroman-4-ol (2a)[19]: Pale orange oil (44% yield). ^{1}H NMR ($CDCl_3$, 400 MHz) δ: 0.97 (s, CH_3, 3H), 1.04 (s, CH_3, 3H), 3.74–3.77 (d, J = 12 Hz, CH_2, 1H), 3.96–3.99 (d, J = 12 Hz, CH2, 1H), 4.26 (s, CH, 1H), 6.82–6.84 (d, J = 8 Hz, Ar, 1H), 6.91–6.95 (t, J = 8 Hz, Ar, 1H), 7.19–7.22 (m, Ar, 1H), 7.32–7.34 (d, J = 8 Hz, Ar, 1H). ^{13}C NMR ($CDCl_3$, 100 MHz) δ: 19.5, 22.6, 33.4, 71.8, 72.4, 116.6, 120.8, 124.2, 129.6, 129.8, 153.6.

5-Methoxy-3,3-dimethylchroman-4-ol (2b)[19]: White solid (18% yield). m.p. = 66.7–68.0oC. ^{1}H NMR ($CDCl_3$, 400 MHz) δ: 0.93 (s, CH_3, 3H), 1.09 (s, CH_3, 3H), 3.65–3.68 (d, J = 12 Hz, CH2, 1H), 3.86 (s, OCH_3, 3H), 3.93–3.95 (d, J = 8 Hz, CH_2, 1H), 4.45 (s, CH, 1H), 6.45–6.52 (m, Ar, 2H), 7.12.7.16 (t, J = 8 Hz, Ar, 1H). ^{13}C NMR ($CDCl_3$, 100 MHz) δ: 20.3, 22.8, 33.1, 55.6, 67.1, 70.9, 102.2, 109.8, 113.3, 129.3, 154.5, 158.9. MS (ESI) *m/z*: 191 $[M]^+$(–OH).

6-Fluoro-3,3-dimethylchroman-4-ol (2c)[19]: Dark brown oil (40 % yield). ^{1}H NMR ($CDCl_3$, 400 MHz) δ: 0.98 (s, CH_3, 3H), 1.02 (s, CH_3, 3H), 3.73–3.76 (d, J = 12 Hz, CH_2, 1H), 3.92–3.94 (d, J = 8 Hz, CH_2, 1H), 4.26 (s, CH, 1H), 6.74–6.78 (m, Ar, 1H), 6.87–6.92 (m, Ar, 1H), 7.04–7.07 (m, Ar, 1H). ^{13}C NMR ($CDCl_3$, 100 MHz) δ: 19.0, 22.6, 29.8, 72.3, 72.4, 115.2–115.4, 116.2–116.4, 117.5–117.5, 125.1–125.2, 149.6–149.7, 155.9–158.3. MS (ESI) *m/z*: 179 $[M]^+$(–OH).

7-Fluoro-3,3-dimethylchroman-4-ol (2d)[19]: Yellow oil (97% yield). ^{1}H NMR ($CDCl_3$, 400 MHz) δ: 0.94 (s, CH_3, 3H), 1.03 (s, CH_3, 3H), 3.73–3.76 (d, J = 12 Hz, CH_2, 1H), 3.95–3.98 (d, J = 12 Hz, CH_2, 1H), 4.21 (s, CH, 1H), 6.52–6.55 (m, Ar, 1H), 6.61–6.66 (m, Ar, 1H), 7.24–7.28 (t, J = 8 Hz, Ar, 1H). ^{13}C NMR ($CDCl_3$, 100 MHz) δ: 19.5, 33.4, 71.9, 71.9, 103.5–103.7, 108.0–108.2, 120.1–120.2, 131.0–131.1, 154.8–154.9, 162.1–164.6. MS (ESI) *m/z*: 219.12 $[M]^+$Na.

6,7-Difluoro-3,3-dimethylchroman-4-ol (2e)[19]: Pale yellow oil (63% yield). ^{1}H NMR ($CDCl_3$, 400 MHz) δ: 0.96 (s, CH_3, 3H), 1.01 (s, CH_3, 3H), 3.73–3.75 (d, J = 8 Hz, CH_2, 1H), 3.91–3.93 (d, J = 8 Hz, CH_2, 1H), 4.21 (s, CH, 1H), 6.60–6.64 (m, Ar, 1H), 7.11–7.16 (m, Ar, 1H). ^{13}C NMR ($CDCl_3$, 100 MHz) δ: 19.0, 33.2, 71.9, 72.3, 105.2–105.4, 117.0–117.2, 119.8–119.9, 143.8–146.4, 149.2–151.8, 149.8–149.9. MS (ESI) *m/z*: 197 $[M]^+$(–OH).

4-Hydroxy-3,3-dimethylchromane-6-carbonitrile (2f)[19]: Pale orange oil (42% yield). ^{1}H NMR ($CDCl_3$, 400 MHz) δ: 0.97 (s, CH_3, 3H), 1.02 (s, CH_3, 3H), 3.83–3.86 (d, J = 12 Hz, CH_2, 1H), 4.00–4.03 (d, J = 12 Hz, CH2, 1H), 4.30 (s, CH, 1H), 6.86–6.88 (d, J = 8 Hz, Ar, 1H), 7.44–7.47 (m, Ar, 1H), 7.68 (s, Ar, 1H). ^{13}C NMR ($CDCl_3$, 100 MHz) δ: 18.9, 22.4, 33.2, 71.6, 72.8, 103.9, 117.6, 119.3, 125.2, 133.2, 134.3, 157.6. MS (ESI) *m/z*: 186 $[M]^+$(–OH).

3,3,6-Trimethylchroman-4-ol (2g)[19]: Pale yellow oil (31% yield). ^{1}H NMR ($CDCl_3$, 400 MHz) δ: 0.96 (s, CH3, 3H), 1.03 (s, CH_3, 3H), 1.73 (s br, OH, 1H), 2.28 (s, CH_3, 3H), 3.71–3.73 (d, J = 8 Hz, CH_2, 1H), 3.93–3.95 (d, J = 8 Hz, CH_2, 1H), 4.21 (s, CH, 1H), 6.72–6.74 (d, J = 8 Hz, Ar, 1H), 6.99–7.02 (m, Ar, 1H), 7.12 (s, Ar, 1H). ^{13}C NMR ($CDCl_3$, 100 MHz) δ: 19.5, 20.6, 22.6, 33.4, 71.7, 72.5, 116.3, 123.8, 130.03, 130.06, 130.3, 151.4. MS (ESI) *m/z*: 175 $[M]^+$(–OH).

8-Ethoxy-4-hydroxy-3,3-dimethylchromane-6-carbonitrile (2h)[19]: Pale orange oil (42% yield). ^{1}H NMR ($CDCl_3$, 400 MHz) δ: 0.96 (s, CH_3, 3H), 1.02 (s, CH_3, 3H), 1.45–1.48 (m, CH_3, 3H), 3.90–3.93 (d, J = 12 Hz, CH_2, 1H), 4.05–4.10 (m, CH_2, 3H), 4.26 (s, CH, 1H), 6.98 (s, Ar, 1H), 7.31–7.32 (m, Ar, 1H). ^{13}C NMR ($CDCl_3$, 100 MHz) δ: 14.6, 19.0, 22.5, 33.0, 64.9, 71.5, 72.9, 103.2, 114.5, 119.4, 125.9, 126.6, 147.65, 147.67. MS (ESI) *m/z*: 248 $[M]^+$.

3,3-Dimethyl-3,4-dihydro-2*H*-benzo[*g*]chromen-4-ol (2i)[19]: Pale brownish solid (32% yield). m.p. = 75.1–77.0 °C. ^{1}H NMR ($CDCl_3$, 400 MHz) δ: 1.03 (s, CH_3, 3H), 1.07 (s, CH_3, 3H), 3.85–3.87 (d, J = 8 Hz, CH2, 1H), 4.09–4.12 (d, J = 12 Hz, CH_2, 1H), 4.52 (s, CH, 1H), 7.21 (s, Ar, 1H), 7.28–7.32 (t, J = 8 Hz, Ar, 1H), 7.38–7.42 (t, J = 8 Hz, Ar, 1H), 7.67–7.69 (d, J = 8 Hz, Ar, 1H), 7.74–7.76 (d, J = 8 Hz, Ar, 1H), 7.87 (s, Ar, 1H). ^{13}C NMR ($CDCl_3$, 100 MHz) δ: 19.1, 22.6, 33.6, 72.5, 73.2, 111.0, 123.7, 126.4, 126.6, 126.72, 127.76, 128.82, 128.89, 134.6, 151.8. MS (ESI) *m/z*: 229 $[M]^+$.

2,2-Dimethyl-2,3-dihydro-1*H*-benzo[*f*]chromen-1-ol (2j)[19]: Yellow solid (11% yield). m.p. = 113.5–116.0 °C. ^{1}H NMR ($CDCl_3$, 400 MHz) δ: 0.96 (s, CH_3, 3H), 1.18 (s, CH_3, 3H), 1.95–1.97 (s br, OH, 1H), 3.78–3.81 (m, CH_2, 1H), 4.07–4.09 (d, J = 8 Hz, CH_2, 1H), 4.71–4.72 (d, J = 4 Hz, CH, 1H), 7.05–7.07 (d, J = 8 Hz, Ar, 1H), 7.35–7.39 (t, J = 8 Hz, Ar, 1H), 7.52–7.56 (t, J = 8 Hz, Ar, 1H), 7.70–7.72 (d, J = 8 Hz, Ar, 1H), 7.76–7.79 (m, Ar, 1H), 8.08–8.10 (d, J = 8 Hz, Ar, 1H). ^{13}C NMR ($CDCl_3$, 100 MHz) δ: 20.9, 22.5, 33.3, 68.2, 70.2, 114.8, 118.8, 122.0, 123.6, 127.2, 128.7, 129.4, 130.4, 133.3, 151.4. **MS (ESI) *m/z*:** 211 $[M]^+$(–OH).

3,3-Dimethyl-3,4-dihydro-2*H*-pyrano[3,2-*h*]quinolin-4-ol (2k)[19]: Brownish oil (57% yield). ^{1}H NMR ($CDCl_3$, 400 MHz) δ: 0.99 (s, CH_3, 3H), 1.09 (s, CH_3, 3H), 4.05–4.07 (d, J = 8 Hz, CH_2, 1H), 4.18–4.21 (d, J = 12 Hz, CH_2, 1H), 4.37 (s, CH, 1H), 7.30–7.32 (d, J = 8 Hz, Ar, 1H), 7.35–7.39 (m, Ar, 1H), 7.47–7.49 (d, J = 8 Hz, Ar, 1H), 8.04–8.06 (d, J = 8 Hz, Ar, 1H), 8.86–8.87 (m, Ar, 1H). ^{13}C NMR ($CDCl_3$, 100 MHz) δ: 19.6, 22.7, 33.4, 72.2, 72.6, 119.3, 121.6, 121.7, 128.0, 129.0, 135.9, 139.4, 149.1, 149.4. MS (ESI) *m/z*: 230 $[M]^+$.

3,3-Dimethylchroman-4-one (3a)[19]: Pale yellow oil (75% yield). ^{1}H NMR ($CDCl_3$, 400 MHz) δ: 1.20 (s, CH_3, 6H), 4.14 (s, CH_2, 2H), 6.94–6.96 (d, J = 8 Hz, Ar, 1H), 6.99–7.03 (t, J = 8 Hz, Ar, 1H), 7.43–7.47 (m, Ar, 1H), 7.88–7.90 (d, J = 8 Hz, Ar, 1H). ^{13}C NMR ($CDCl_3$, 100 MHz) δ: 20.5, 41.7, 76.7, 117.7, 119.6, 121.5, 127.8, 135.6, 161.2, 197.4.

5-Methoxy-3,3-dimethylchroman-4-one (3b)[19]: Pale yellow solid (35% yield). m.p. = 51.9–53.0 °C. ^{1}H NMR ($CDCl_3$, 400 MHz) δ: 1.18 (s, CH_3, 6H), 3.89 (s, OCH_3, 3H), 4.09 (s, CH_2, 2H), 6.50–6.56 (m, Ar, 2H), 7.33–7.37 (t, J = 8 Hz, Ar, 1H). ^{13}C NMR ($CDCl_3$, 100 MHz) δ: 20.8, 42.3, 56.2, 76.2, 103.9, 109.8, 135.6, 161.4, 163.0, 196.3. MS (ESI) *m/z*: 207 $[M]^+$.

6-Fluoro-3,3-dimethylchroman-4-one (3c)[19]: Pale yellow oil (35% yield). **^{1}H NMR** ($CDCl_3$, 400 MHz) δ: 1.20 (s, CH3, 6H), 4.13 (s, CH_2, 2H), 6.92–6.96 (m, Ar, 1H), 7.16–7.21 (m, Ar, 1H), 7.53–7.55 (m, Ar, 1H). **^{13}C NMR ($CDCl_3$, 100 MHz) δ**: 20.5, 41.7, 76.9, 112.6–112.8, 119.3–119.4, 123.1–123.4, 156.2, 157.50–157.51, 158.6, 196.6–196.7.

7-Fluoro-3,3-dimethylchroman-4-one (3d)[19]: Pale yellow solid (22% yield). **m.p.** = 51.3–52.9 °C. ^{1}H NMR ($CDCl_3$, 400 MHz) δ: 1.38 (s, CH_3, 6H), 3.81 (s, CH_2, 2H), 6.58–6.64 (m, Ar, 2H), 7.46–7.49 (m, Ar, 1H). ^{13}C NMR ($CDCl_3$, 100 MHz) δ: 26.1, 70.2, 77.4, 101.6–101.9, 106.6–106.7, 108.8–109.1, 133.5–133.6, 155.9–156.0, 161.5–164.0,

196.1. MS (ESI) *m/z*: 219 $[M]^+Na$.

6,7-Difluoro-3,3-dimethylchroman-4-one (3e)[19]: Brownish oil (41% yield). ^1H NMR ($CDCl_3$, 400 MHz) δ: 1.19 (s, CH3, 6H), 4.14 (s, CH2, 2H), 6.75–6.79 (m, Ar, 1H), 7.64–7.69 (m, Ar, 1H). ^{13}C NMR ($CDCl_3$, 100 MHz) δ: 20.6, 41.4, 106.3, 106.5, 114.9, 115.1, 115.7, 144.8, 144.9,147.2, 147.3,153.7, 153.8, 156.3, 156.4, 157.9, 158.1, 195.3. MS (ESI) *m/z*: 212 $[M]^+$.

8-Ethoxy-3,3-dimethyl-4-oxochromane-6-carbonitrile (3f)[19]: Yellow solid (42% yield). m.p. = 90.3–92.9 °C. ^1H NMR ($CDCl_3$, 400 MHz) δ: 1.21 (s, CH_3, 6H), 1.49–1.53 (t, J = 8 Hz, CH_3, 3H), 4.09–4.15 (q, J = 8 Hz, CH2, 2H), 4.29 (s, CH2, 2H), 7.16 (s, Ar, 1H), 7.82 (s, Ar, 1H). ^{13}C NMR ($CDCl_3$, 100 MHz) δ: 14.5, 20.3, 41.5, 65.3, 77.4, 104.7, 118.2, 118.4, 120.2, 124.4, 148.8, 154.5, 195.3. MS (ESI) *m/z*: 246 $[M]^+$.

3,3-Dimethyl-2,3-dihydro-4*H*-benzo [*g*] chromen-4-one (3g)[19]: Pale orange oil (80% yield). ^1H NMR ($CDCl_3$, 400 MHz) δ: 1.29 (s, CH_3, 6), 4.21 (s, CH_2, 2H), 7.34–7.38 (t, J = 8 Hz, Ar, 2H), 7.49–7.53 (t, J = 8 Hz, Ar, 1H), 7.71–7.73 (d, J = 8 Hz, Ar, 1H), 7.88–7.90 (d, J = 8 Hz, Ar, 1H), 8.54 (s, Ar, 1H). ^{13}C NMR ($CDCl_3$, 100 MHz) δ: 20.5, 42.5, 76.4, 112.3, 120.4, 124.5, 126.5, 128.5, 129.0, 129.8, 137.6, 156.6, 197.8. HRMS (ESI): *m/z* calculated for $C_{15}H_{14}O_2$ $[M + H]^+$: 227.10718, found 227.10665.

2,2-Dimethyl-2,3-dihydro-1*H*-benzo [*f*] chromen-1-one (3h)[19]: Pale yellow oil (91% yield). ^1H NMR ($CDCl_3$, 400 MHz) δ: 1.26 (s, CH_3, 6H), 4.26 (s, CH_2, 2H), 7.08–7.10 (d, J = 8 Hz, Ar, 1H), 7.40–7.44 (t, J = 8 Hz, Ar, 1H), 7.61–7.65 (t, J = 8 Hz, Ar, 1H), 7.74–7.76 (d, J = 8 Hz, Ar, 1H), 7.90–7.92 (d, J = 8 Hz, Ar, 1H), 9.48–9.50(s, Ar, 1H). ^{13}C NMR ($CDCl_3$, 100 MHz) δ: 21.0, 42.0, 76.5, 110.9, 118.6, 124.7, 125.9, 128.4, 129.4, 129.5, 132.0, 137.1, 163.0, 198.6.

3,3-Dimethyl-2,3-dihydro-4*H*-pyrano [3,2-*h*] quinolin-4-one (3i)[19]: Pale yellow oil (93% yield). ^1H NMR ($CDCl_3$, 400 MHz) δ: 1.27 (s, CH_3, 6H), 4.47 (s, CH_2, 2H), 7.38–7.40 (d, J = 8 Hz, Ar, 1H), 7.51–7.54 (m, Ar, 1H), 7.96–7.98 (d, J = 8 Hz, Ar, 1H), 8.11–8.14 (m, Ar, 1H), 8.96–8.97 (m, Ar, 1H). ^{13}C NMR ($CDCl_3$, 100 MHz) δ: 20.7, 41.3, 77.8, 116.9, 120.3, 123.6, 124.0, 132.7, 136.2, 140.1, 150.2, 158.5, 197.2.

3,3-Dimethyl-2,3-dihydro-4*H*-pyrano [2,3-*b*] pyridin-4-one (3j)[19]: Pale yellow solid (41% yield). m.p. = 53.0–55.9 °C. ^1H NMR ($CDCl_3$, 400 MHz) δ: 1.21 (s, CH_3, 6H), 4.25 (s, CH_2, 2H), 7.06–7.09 (m, Ar, 1H), 8.24–8.26 (d, J = 8 Hz, Ar, 1H), 8.44–8.45 (m, Ar, 1H). ^{13}C NMR ($CDCl_3$, 100 MHz) δ: 20.4, 41.5, 75.8, 114.2, 118.7, 137.9, 154.6, 165.5, 197.0. MS (ESI) *m/z*: 178 $[M]^+$.

3,3-Dimethyl-8-(trifluoromethoxy)chroman-4-one (3k): pale yellow oil (38% yield).[1]H NMR ($CDCl_3$, 400 MHz) **δ**: 1.20 (s, CH_3, 6H), 4.17 (s, CH_2, 2H), 6.80 (s, CH, Ar,1H), 6.84–6.86 (d, J = 8 Hz, Ar, 1H),7.92–7.94 (d, J = 8 Hz, Ar, 1H).[13]C NMR ($CDCl_3$, 100 MHz) δ: 20.3, 41.6, 108.9, 113.6, 116.3, 117.8, 118.9, 121.5 (q, J = 258 Hz), 124.1 129.8, 154.3, 162.1, 195.9. HRMS (ESI): calculated for $C_{12}H_{11}F_3O_3$ $[M + H]^+$: 261.0738, found 261.0733.

8-Methoxy-3,3-dimethylchroman-4-one (3l): pale yellow oil (78 % yield).[1]H NMR ($CDCl_3$, 400 MHz) δ: 1.20 (s, CH_3, 6H), 3.90 (s, CH_3, 3H), 4.23 (s, CH_2, 2H), 6.93–6.97 (t, J = 8 Hz, Ar, 1H),7.03–7.04 (d, J = 4 Hz, Ar, 1H), 7.48–7.50 (d, J = 8 Hz, Ar, 1H).[13]C NMR ($CDCl_3$, 100 MHz) δ: 20.4, 41.5, 56.1, 77.1, 116.1, 118.8, 120.0, 120.9, 148.5, 150.9, 197.2. HRMS (ESI): calculated for $C_{12}H_{14}O_3$ $[M + H]^+$: 207.1021, found: 207.1015.

3,3,6-Trimethylchroman-4-one (3m)[19]: Colorless oil; mixture of substrate (**1g**) and ketone (**3m**), impossible to separate by silica gel chromatography. ^1H NMR ($CDCl_3$, 400 MHz) δ: 1.19 (s, CH_3, 6H), 2.26 (s, CH_3, 3H), 4.11 (s, CH_2, 2H), 6.84-6.86 (d, J = 8 Hz, Ar, 1H),7.25-7.28 (m, Ar, 1H), 7.68 (s, Ar, 1H). ^{13}C NMR ($CDCl_3$, 100 MHz) δ: 20.53, 20.62, 41.73, 76.77, 117.51, 119.19, 127.38, 130.94, 136.76, 159.29, 197.65.

5.1.3. General Procedure for the synthesis of chroman-4-amine derivatives

To a solution of the chromanone substrate (**3**) (1 mmol) in EtOH (3 mL), in an Ace® pressure flash was added 25% aqueous ammonia (5mL), ammonium acetate (20 equivalents) and sodium cyanoborohydride (2.5 equivalents). The mixture was allowed to stir at 120 °C for several hours, monitored by TLC. After consumption of the substrate, the mixture was cooled to room temperature followed by removal of ethanol under reduced pressure. Then, aqueous NaOH (2 M) solution was added to the crude mixture until pH = 10–12, then, the solution was extracted with AcOEt. The organic phase was dried, and the solvent was evaporated. Flash chromatography was performed using AcOEt/Hexane (2/1) as eluent furnishing the desired compound.

3,3-Dimethylchroman-4-amine (4a): pale yellow oil (57% yield). ^1H NMR ($CDCl_3$, 400 MHz) δ: 0.96 (s, CH_3, 3H), 0.97 (s, CH_3,3H), 1.77 (s, NH_2, 2H), 3.59 (s, CH, 1H), 3.72–3.75 (d, J = 12 Hz, CH, 1H), 3.95–3.98 (d, J = 12 Hz, CH, 1H), 6.78–6.80 (d, J = 8 Hz, Ar, 1H), 6.89–6.92 (m, Ar, 1H), 7.12–7.16 (t, J = 8 Hz, Ar, 1H), 7.35–7.36 (d, J = 4 Hz, Ar, 1H).[13]C NMR ($CDCl_3$, 100 MHz) δ: 19.1, 23.4, 32.8, 55.2, 72.6, 116.2, 120.5, 125.6, 128.3, 129.1, 153.5. HRMS (ESI): calculated for $C_{11}H_{15}NO$ $[M + H]^+$: 178.1232, found: 178.1226.

8-Methoxy-3,3-dimethylchroman-4-amine (4b): pale yellow oil (81% yield). ^1H NMR ($CDCl_3$, 400 MHz) δ: 0.97 (s, CH_3, 3H), 0.98 (s, CH_3,3H), 1.50 (s, NH_2, 2H), 3.58 (s, CH, 1H), 3.81–3.83 (d, J = 8 Hz, CH, 1H), 3.86 (s, CH_3, 3H), 4.03–4.06 (d, J = 12 Hz, CH, 1H), 6.75–6.77 (d, J = 8 Hz, Ar, 1H), 6.84–6.88 (t, J = 8 Hz, Ar, 1H), 6.95–6.97 (d, J = 8 Hz, Ar, 1H).[13]C NMR ($CDCl_3$, 100 MHz) δ: 19.2, 23.4, 32.7, 55.1, 55.8, 72.9, 109.7, 120.1, 120.8, 126.6, 142.8, 147.8. HRMS (ESI): calculated for $C_{12}H_{17}NO_2$ $[M + H]^+$: 208.1337, found 208.1332.

3,3,6-Trimethylchroman-4-amine (4c): pale yellow oil (74% yield). ^1H NMR ($CDCl_3$, 400 MHz) δ: 0.96 (s, CH_3, 3H), 0.97 (s, CH_3, 3H), 1.77 (s, NH_2, 2H), 2.27 (s, CH_3, 3H), 3.56 (s, CH, 1H), 3.70–3.73 (d, J = 12 Hz, CH, 1H), 3.91–3.94 (d, J = 12 Hz, CH, 1H), 6.69–6.71 (d, J = 8 Hz, Ar, 1H), 6.94–6.96 (d, J = 8 Hz, Ar, 1H), 7.16 (s, Ar, 1H).[13]C NMR ($CDCl_3$, 100 MHz) δ: 18.0, 19.5, 22.4, 31.8, 54.3, 71.6, 114.9, 124.5, 127.9, 128.3, 128.6, 150.2. HRMS (ESI): calculated for $C_{12}H_{17}NO$ $[M-(NH_2)]^+$: 175.1123, found 175.1115.

3,3-Dimethyl-3,4-dihydro-2H-benzo [*g*] chromen-4-amine (4d): pale yellow oil (72% yield). ^1H NMR ($CDCl_3$, 400 MHz) δ: 1.00 (s, CH_3, 3H), 1.06 (s, CH_3, 3H), 1.58 (s, NH_2, 2H), 3.85 (s, CH, 1H), 3.88–3.90 (d, J = 8 Hz, CH, 1H), 4.10–4.12 (d, J = 8 Hz, CH, 1H), 7.21 (s, Ar, 1H), 7.28–7.33 (m, Ar, 1H), 7.38–7.42 (t, J = 8 Hz, Ar, 1H), 7.69–7.71 (d, J = 8 Hz, Ar, 1H), 7.76–7.78 (d, J = 8 Hz, Ar, 1H), 7.95 (s, Ar, 1H),[13]C NMR ($CDCl_3$, 100 MHz) δ:18.5, 23.3, 33.1, 56.2, 73.6, 110.6, 123.3, 126.0, 126.2, 127.4, 127.8, 128.3, 128.8, 133.9, 152.2. HRMS (ESI): calculated for $C_{15}H_{17}NO$ $[M + H]^+$: 228.1388, found: 228.1382.

2,2-Dimethyl-2,3-dihydro-1H-benzo [*f*] chromen-1-amine (4e): pale yellow oil (76% yield). ^1H NMR ($CDCl_3$, 400 MHz) δ: 0.98 (s, CH_3, 3H), 1.12 (s, CH_3, 3H), 1.89 (s, NH_2, 2H), 3.71–3.74 (d, J = 12 Hz, CH, 1H), 4.07 (s, CH, 1H), 4.19–4.22 (d, J = 8 Hz, CH, 1H), 7.03–7.06 (d, J = 12 Hz, Ar, 1H), 7.32–7.36 (t, J = 8 Hz, Ar, 1H), 7.50–7.54 (t, J = 8 Hz, Ar, 1H), 7.65–7.68 (d, J = 12 Hz, Ar, 1H), 7.76–7.78 (d, J = 8 Hz, Ar, 1H), 8.02–8.04 (d, J = 12 Hz Ar, 1H). ^{13}C NMR ($CDCl_3$, 100 MHz) δ: 20.3, 22.5, 31.5, 49.7, 68.6, 115.4, 117.7, 120.6, 122.0, 125.7, 127.7, 128.0, 128.3, 132.0, 149.7. HRMS (ESI): calculated for $C_{15}H_{17}NO$ $[M-(NH_2)]^+$: 211.1123, found: 211.1113.

Chroman-4-amine (4f)[29]**: ^1H NMR ($CDCl_3$, 400 MHz) δ**: White solid (40% yield). 1.80–1.87 (m, NH_2,CH,3H), 2.12–2.19 (m, CH, 1H), 4.02–4.05 (m, CH, 1H), 4.19–4.30 (m, CH_2, 2H), 6.80–6.82 (d, J = 8 Hz, Ar, 1H), 6.88–6.92 (t, J = 8 Hz, Ar, 1H), 7.12–7.16 (t, J = 8 Hz, Ar, 1H), 7.29–7.30 (d, J = 8 Hz, Ar, 1H). ^{13}C NMR ($CDCl_3$, 100 MHz) δ: 32.0, 45.0, 62.7, 116.9, 120.5, 126.4, 128.5, 128.8, 154.2. MS (ESI) *m/z*: 133.07 $[M-(NH_2)]^+$, 133.09.

5.1.4. General Procedure for the propargylation of chroman-4-amine derivatives

Under a nitrogen atmosphere, the chroman-4-amine derivative (**4a**), (**4b**) and (**4c**) (0.56 mmol) was added to a round bottom flask, then dissolved in dry DMF (4 mL). Sodium hydride (1.3 equivalents) was added to the reaction mixture and left to stir for 30 mins followed by

dropwise addition of a solution of propargyl bromide (1.5 equivalents). The reaction mixture was allowed to stir for 24 h, at room temperature. After total consumption of the starting material, a saturated solution of NH_4Cl was added, and the organic phase was extracted with Et_2O and dried using anhydrous magnesium sulfate. Concentration under reduced pressure, followed by flash chromatography delivered the desired compound.

3,3-Dimethyl-*N*-(prop-2-yn-1-yl)chroman-4-amine (5a): pale yellow oil (65% yield). ^{1}H NMR ($CDCl_3$, 400 MHz) δ: 0.93 (s, CH_3, 3H), 1.02 (s, CH_3, 3H), 1.42 (s, NH, 1H), 2.37(s, CH, 1H), 3.44 (s, CH, 1H), 3.50 (s, CH_2, 2H), 3.65–3.68(d, J = 8 Hz, CH, 1H), 4.04–4.07 (d, J = 12 Hz, CH, 1H), 6.79–6.82 (d, J = 12 Hz, Ar, 1H), 6.86–6.90 (t, J = 8 Hz, Ar, 1H), 7.14–7.18 (t, J = 8 Hz, Ar, 1H), 7.31–7.33(d, J = 8 Hz, Ar, 1H). ^{13}C NMR ($CDCl_3$, 100 MHz) δ: 21.2, 23.6, 33.3, 38.1, 59.3, 71.4, 71.7, 83.1, 116.4, 120.1, 123.6, 128.7, 130.7, 153.3. HRMS (ESI): calculated for $C_{14}H_{17}NO$ $[M + H]^+$: 216.1388, found: 216.1382.

8-Methoxy-3,3-dimethyl-*N*-(prop-2-yn-1-yl)chroman-4-amine (5b): pale yellow oil (75% yield). ^{1}H NMR ($CDCl_3$, 400 MHz) δ:0.94 (s, CH_3, 3H), 1.02 (s, CH_3, 3H), 1.49 (s, NH, 1H), 2.33 (s, CH, 1H), 3.43 (s, CH, 1H), 3.50–3.52(d, J = 8 Hz, CH_2, 2H), 3.78–3.81 (d, J = 12 Hz, CH, 1H), 3.86 (s, CH_3, 3H), 4.08–4.10 (d, J = 8 Hz, CH,1H), 6.76–6.78 (d, J = 8 Hz, Ar, 1H), 6.82–6.86 (t, J = 8 Hz, Ar, 1H), 6.95–6.97 (d, J = 8 Hz, Ar, 1H). ^{13}C NMR ($CDCl_3$, 100 MHz) δ: 20.5, 22.5, 32.3, 37.3, 54.8, 58.2, 70.7, 75.6, 82.0, 109.0, 118.7, 121.3, 123.3, 141.7, 147.0. HRMS (ESI): calculated for $C_{15}H_{19}NO_2$ $[M + H]^+$: 246.1494, found 246.1486.

3,3,6-Trimethyl-*N*-(prop-2-yn-1-yl)chroman-4-amine (5c): pale yellow oil (53% yield). ^{1}H NMR ($CDCl_3$, 400 MHz) δ: 0.93 (s, CH_3, 3H), 1.01 (s, CH_3, 3H), 1.56 (s, NH, 1H), 2.27 (s, CH, 1H), 2.34 (s, CH_3, 3H), 3.38 (s, CH, 1H), 3.51–3.53(t, J = 4 Hz, CH_2, 2H), 3.62–3.64 (d, J = 8 Hz, CH, 1H), 4.00–4.03(d, J = 8 Hz, CH,1H), 6.69–6.71 (d, J = 8 Hz, Ar, 1H), 6.95–6.97 (d, J = 8 Hz, Ar, 1H), 7.10 (s, Ar, 1H).[13]C NMR ($CDCl_3$, 100 MHz) δ: 22.5, 23.3, 33.8, 39.9, 57.1, 70.6, 72.0, 115.1, 118.8, 121.7, 123.1, 126.7, 128.8, 129.4, 132.9. HRMS (ESI): calculated for $C_{15}H_{19}NO$ $[M + H]^+$: 230.1545, found 230.1536.

5.1.5. General Procedure for the benzylation of N-(prop-2-yn-1-yl) chroman-4-amine derivatives

The corresponding *N*-(prop-2-yn-1-yl) chroman-4-amine derivative (**5a**) or (**5b**), was dissolved in dry DMF (2 mL), followed by addition of K_2CO_3 (1.2 equivalents). The reaction mixture was allowed to stir for 1 h, then benzyl bromide (1.2 equivalents) was added. The reaction was heated to 100 °C. After consumption of the starting material, the reaction mixture was allowed to cool, then diluted with H_2O (5 mL). The organic phase was extracted with Et_2O and dried with anhydrous magnesium sulfate. After evaporation of the solvent under reduced pressure, and flash chromatography purification the final product was obtained.

***N*-Benzyl-3,3-dimethyl-*N*-(prop-2-yn-1-yl)chroman-4-amine (5d):** pale yellow oil (63% yield). ^{1}H NMR ($CDCl_3$, 400 MHz) δ: 1.01 (s, CH_3, 3H), 1.22 (s, CH_3, 3H), 2.38 (s, NH, 1H), 3.41 (s, CH, 1H), 3.49–3.60 (q, J = 16 Hz, CH_2, 2H), 3.77–3.79 (d, J = 8 Hz CH, 1H), 4.15–4.17(d, J = 8 Hz, CH, 1H), 6.88–6.90 (d, J = 8 Hz, Ar, 1H), 6.97–7.01(t, J = 8 Hz, Ar,1H), 7.22–7.29 (m, Ar, 2H), 7.32–7.38 (q, J = 8 Hz, Ar, 4H), 7.45–7.47(d, J = 8 Hz, Ar, 1H).[13]C NMR ($CDCl_3$, 100 MHz) δ: 20.7, 23.1, 34.2, 42.1, 52.3, 55.0, 63.3, 70.60, 71.5, 80.5, 115.3, 118.7, 119.4, 125.9, 127.2, 127.4, 127.7, 130.7, 138.9, 153.0. HRMS (ESI): calculated for $C_{21}H_{23}NO$ $[M + H]^+$: 306.1858, found 306.1848.

***N*-Benzyl-8-methoxy-3,3-dimethyl-*N*-(prop-2-yn-1-yl)chroman-4-amine (5e):** pale yellow oil (70 % yield). ^{1}H NMR ($CDCl_3$, 400 MHz) δ: 0.98 (s, CH_3, 3H), 1.18 (s, CH_3, 3H), 1.59 (s, NH, 1H), 2.34 (s, CH, 1H), 3.35–3.36 (d, J = 4 Hz CH_2, 2H), 3.44–3.55 (m, CH_2, 2H), 3.75 (s, CH, 1H), 3.90 (s, CH_3, 3H), 4.16–4.19 (d, J = 12 Hz, CH, 1H), 6.81–6.83(d, J = 8 Hz, CH,1H), 6.88–6.92 (t, J = 8 Hz Ar, 1H), 7.03–7.05 (d, J = 8 Hz, Ar, 1H), 7.23–7.31(m, Ar, 5H).[13]C NMR ($CDCl_3$, 100 MHz) δ: 20.7, 23.1, 28.6, 29.9, 34.1, 42.0, 54.7, 63.1, 70.8, 71.5, 80.5, 108.9, 118.2, 120.1, 122.5, 125.9, 127.2, 127.4, 138.9, 142.3, 146.9. HRMS (EI) calculated for $C_{22}H_{25}NO_2$ $[M + Na]^+$: 358.1783, found 358.1776.

5.2. Bioassays

5.2.1. – Cholinesterase inhibition

The inhibitory activities of title compounds against commercially available cholinesterases (*ee*AChE) (*Electrophorus electricus*, Type V-S), *eq*BuChE (equine serum)) were conducted using minor modifications of Ellman's assay[30] in a double-beam Hitachi U-2900 spectrophotometer, using 2 mL-PS cuvettes. Reactions were performed in 50 μM phosphate buffer (pH 8.0) in the presence of 0.975 mM DTNB (Ellman's reagent); stock inhibitors solutions were prepared in DMSO, and the solvent was kept at 1.25% concentration in the cuvette.

A preliminary screening was conducted using a 100 μM inhibitor concentration and [S] = K_M (121 μM for AChE and 112 μM for BuChE). Substrates were commercially available acetylthiocholine and S-butyrylthiocholine iodides. The enzyme was dissolved in water in such a concentration so as to keep the reaction rate within 0.12–0.15 Abs/min at the highest substrate concentration used in the experiment (4 × K_M). Reactions (in the presence and in the absence of inhibitors) were initiated by the addition of the enzyme and monitored (T = 25 °C) for 125 s at 405 nm.

For those compounds showing %I > 50% at 100 μM concentration, IC_{50} values were calculated by plotting %I vs. log[I] (4–6 different inhibitor concentrations) using a second-order equation fit; data were obtained in duplicate, and are expressed as average ± SD. For IC_{50} < 10 μM, inhibition constants (Ki's) and mode of inhibition were obtained; for this purpose, 5 different substrate concentrations (1/4 × K_M to 4 × K_M) and 3–4 different inhibitor concentrations (giving roughly 30–80% inhibition) were used. Kinetic parameters (K_M, V_{max}) were obtained using a nonlinear regression analysis (GraphPad Prism 8.01). Mode of inhibition was obtained using the Cornish-Bowden plots (1/v vs. [I], [S]/v vs. [I]).[31]

For the mixed-type inhibition observed for the strongest inhibitors herein, Ki's were calculated using the following equations:

$$K_{M,app} = K_M \frac{1 + \frac{[I]}{K_{ia}}}{1 + \frac{[I]}{K_{ib}}}$$

$$V_{max,app} = \frac{V_{max}}{1 + \frac{[I]}{K_{ia}}}$$

$K_{M,app}$ = Apparent K_M; $V_{max,app}$ = apparent V_{max}; K_{ia} = inhibitory constants for the inhibitor binding the free enzyme; K_{ib} = inhibitory constant for the inhibitor binding the E-S complex.

5.2.2. – Monoamine oxidase inhibition

One-point screening of monoamine oxidases was conducted for both MAO-A and B isoforms. A discontinuous fluorimetric assay was conducted to determine inhibition of MAO-A and B as described previously.[32] The substrate Kynuramine was used for recombinant membrane-bound MAO-A and MAO-B (Sigma-Aldrich, MO, USA) at two-fold K_M concentration (K_M = 30 μM for MAO-A and K_M = 20 μM for MAO-B). The mixture in a total volume of 100 μL was pipetted onto flat-bottomed black 96-well plates (No. 655076, greiner bio-one GmbH, Austria). This procedure was partially automated using an EVO freedom pipetting robot (Tecan Trading AG, Switzerland). The enzyme reaction was stopped after 20 min incubation (37 °C) by addition of 35 μL sodium hydroxide (2 N). The remaining enzyme activity was determined by detection of 4-hydroxyquinoline (λ_{Ex} = 320 nm, λ_{Em} = 405 nm) using an infinite M1000 Pro microplate reader (Tecan Trading AG, Switzerland). Product formation in the absence of inhibitor was used as control to calculate the percentage of inhibition at a test concentration of 1 μM. At

least two independent experiments were performed in duplicate and reported as mean ± standard deviation (%) using clorgyline and safinamide as references.

5.3. – Saturation Transfer difference (STD) NMR

The NMR spectroscopy experiments were performed on a Bruker Avance III 400 MHz spectrometer equipped with a 5 mm broadband (PABBO BB/19F-1H/D Z-GRD) resonance probe head. NMR and STD-NMR experiments were carried out with solvent suppression and a 10 ms spinlock filter after the 90° pulse to reduce residual signals from the protein. For selective saturation, cascades of Gaussian pulses with a length of 50 ms and 40–60 dB of attenuation were employed, with an interpulse delay of 1 ms.[24] The on-resonance and off-resonance frequencies were set to 0 and 12000 Hz, respectively. STD-NMR controls were performed using the ligand itself. Blank experiments were performed to guarantee the absence of direct saturation of the ligand proton signals. The relaxation delay was properly adjusted so that the experiment time length was kept constant at 6.5 s. Water suppression at 1880 Hz (4.7 ppm) was conducted. A sweep-width of 8012.82 Hz (20.03 ppm) was employed. Specifically, the saturation time to obtain the STD buildup curves were recorded at 0.25, 0.5, 1, 2, 3, 4, and 5 s.[24]

A 5 μM *eq*BuChE (*equine*) solution was prepared in a D_2O. 8.8 mM and 4.8 mM stock solutions were prepared for compound (**3h**) and (**4b**), respectively. Samples for NMR analysis were prepared by adding 100 μL of the ligand to a500 μL enzyme solutions.

5.4. Molecular modelling

5.4.1. Cholinesterases

All molecular modelling studies were executed by means of the Schrödinger Suite version 2018–1[33] and Maestro GUI[34] was used to build the 3D theoretical structures of all our derivatives. The *h*ChEs recognition was explored by means of molecular docking experiments. Particularly, high-resolution Protein Data Bank (PDB)[35] human crystallographic structures in non-covalent complexes with known inhibitors available, deposited with codes 4EY7[36] and 5NN0[37], were adopted as receptor models of *h*AChE and *h*BuChE isoforms respectively. Because the limits of the PDB file format, both structures were manipulated before to be taken into account as receptors in our docking simulations: missing atoms and bond order were fixed, hydrogen atoms were added, and co-crystallized water solvent molecules and ligands were deleted. After such pre-treatments, Glide[33] algorithm was applied to obtain ligands configurations in the enzymatic binding pockets using a box of about 27,000 $Å^3$ centred on the catalytic serine residues. Ligands structural flexibility was taken into account by the corresponding software implementation sampling a maximum of 10 docking configurations for ligand. The binding affinity was estimated by means of the Standard Precision (SP) scoring function and the top ranked complexes according to Glide Score were considered for the binding modes graphical analysis.

5.4.2. MAO-B

The docking study was executed by means of the Schrödinger Suite version 2018–1[33] and Maestro GUI[34] was used to build the 3D theoretical structure of our ligand. The high-resolution Protein Data Bank (PDB) human crystallographic model deposited with code 6FW0[38], was adopted as receptor models of *h*MAO-B. Taking into account the limits of the PDB file format, the target structure was handled prior to be considered as receptor in our docking computation: missing atoms and FAD bond order were fixed, hydrogen atoms were added. However, the co-crystallized water solvent molecules and the ligand chlorophenyl-chromone-carboxamide were erased. After such pre-treatments, the Glide algorithm was used to generate ligand configurations in the enzymatic cleft using a box of about 64,000 $Å^3$ centred on the FAD N5 atom. Ligand structural flexibility was taken into account by the corresponding software implementation sampling a maximum of 10 docking configurations. The binding affinity was estimated by means of the Standard Precision (SP) scoring function and the complexes were ranked according to the Glide Score.

Declaration of Competing Interest

The authors declare that they have no known competing financial interests or personal relationships that could have appeared to influence the work reported in this paper.

Acknowledgements

We acknowledge the Fundação para a Ciência e a Tecnologia (FCT) for funding through the strategic project to LAQV-REQUIMTE (UIDB/50006/2020). O.L. and J.G.F.-B. thank Grant PID2020-116460RB-I00 funded by MCIN/AEI/10.13039/501100011033 and Junta de Andalucía (FQM-134) for financial support. We are extremely grateful to COST Action 15135, Multi-target paradigm for innovative ligand identification in the drug discovery process (MuTaLig). We thank Dr. César Raposo from the Analytical Services laboratory at the University of Salamanca for the mass spectrometry analyses.

Appendix A. Supplementary data

Supplementary data to this article can be found online at https://doi.org/10.1016/j.bmc.2022.116807.

References

1 (a) WHO, Dementia, 2020. https://www.who.int/news-room/fact-sheets/detail/dementia. Accessed 30 December 2021. (b) Patterson C. World Alzheimer Report 2018: The state of the art of dementia research: New frontiers; Sep 2018. (c) Gauthier S, Rosa-Neto P, Morais J.A, Webster C. World Alzheimer Report 2021: Journey through the diagnosis of dementia. London, England: Alzheimer's Disease International; 2021.

2 Paudel P, Seong SH, Zhou Y, et al. Anti-Alzheimer's Disease Activity of Bromophenols from a *Red Alga*, Symphyocladia latiuscula (Harvey) Yamada. *ACS Omega.* 2019;4:12259–12270. https://doi.org/10.1021/acsomega.9b01557.

3 Proschak E, Stark H, Merk D. Polypharmacology by Design: A Medicinal Chemist's Perspective on Multitargeting Compounds. *J Med Chem.* 2019;62:420–444. https://doi.org/10.1021/acs.jmedchem.8b00760.

4 Marques CS, López Ó, Bagetta D, et al. *N*-1,2,3-triazole-isatin derivatives for cholinesterase and β-amyloid aggregation inhibition: A comprehensive bioassay study. *Bioorg Chem.* 2020;98(103753). https://doi.org/10.1016/j.bioorg.2020.103753.

5 Totobenazara J, Bacalhau P, San Juan AA, et al. Design, Synthesis and Bioassays of 3-Substituted-3-Hydroxyoxindoles for Cholinesterase Inhibition. *Chem Select.* 2016;1:3580–3588. https://doi.org/10.1002/slct.201600932.

6 Maher P. The Potential of Flavonoids for the Treatment of Neurodegenerative Diseases. *Int. J. Mol. Sci.* 2019;20:3056. https://doi.org/10.3390/ijms20123056.

7 a) Pettersson M, Johnson D.S, Rankic D.A, et al. Discovery of cyclopropyl chromane-derived pyridopyrazine-1,6-dione γ-secretase modulators with robust central efficacy.*MedChemComm*. 2017; 8:730–743. 10.1039/c6md00406g b) Singh M, Kaur M, Singh N, Silakari O. Exploration of multi-target potential of chromen-4-one based compounds in Alzheimer's disease: Design, synthesis and biological evaluations. *Bioorg Med Chem.* 2017; 26:4360–4361. 10.1016/j.bmc.2017.09.012 c) Wallace T.W, Saengchantara S.T. Chromanols, chromanones, and chromones *Nat Prod Rep* 1986; 3:465-475. 10.1039/NP9860300465 d) Ellis G.P. Chromenes, Chromanones, and Chromones, Chemistry of Heterocyclic Compounds. vol 100. John Wiley & Sons; 2009. e) Emami S, Ghanbarimasir Z. Recent advances of chroman-4-one derivatives: synthetic approaches and bioactivities. *Eur J Med Chem*. 2015; 93:539-563. 10.1016/j.ejmech.2015.02.048.

8 Liu Q, Qiang X, Li Y, et al. Design, synthesis and evaluation of chromone-2-carboxamido-alkylbenzylamines as multifunctional agents for the treatment of Alzheimer's disease. *Bioorg Med Chem.* 2015;23:911–923. https://doi.org/10.1016/j.bmc.2015.01.042.

9 Jiang N, Ding J, Liu J, et al. Novel chromanone-dithiocarbamate hybrids as multifunctional AChE inhibitors with β-amyloid anti-aggregation properties for the treatment of Alzheimer's disease. *Bioorg Chem.* 2019;89(103027). https://doi.org/10.1016/j.bioorg.2019.103027.

10 Fridén-Saxin M, Seifert T, Landergren MR, et al. Synthesis and Evaluation of Substituted Chroman-4-one and Chromone Derivatives as Sirtuin 2-Selective Inhibitors.*J. Med Chem.* 2012;55(7104–7113). https://doi.org/10.1021/jm3005288.

11 Chin K.-Y, Tay S.S. A Review on the Relationship between Tocotrienol and Alzheimer Disease. *Nutrients*. 2018; 10:881 10.3390/nu10070881.

12 Carradori S, Silvestri R. New Frontiers in Selective Human MAO-B Inhibitors. *J Med Chem.* 2015;58:6717–6732. https://doi.org/10.1021/jm501690r.

13 Lan J-S, Xie S-S, Huang M, et al. Chromanones: selective and reversible monoamine oxidase B inhibitors with nanomolar potency. *MedChemComm*. 2015;6:1293–1302. https://doi.org/10.1039/C5MD00124B.

14 a) Voight E.A, Daanen J.F, Hannick S.M, Shelat B.H, Kerdesky F.A, Plata D.J, Kort M. E. Efficient and general asymmetric syntheses of (R)-chroman-4-amine salts. *Tetrahedron Lett.* 2010; 51:5904–5907. 10.1016/j.tetlet.2010.09.006 b) Lloyd J, Atwal K.S, Finlay H.J, Nyman M, Huynh T, Bhandaru R, Kover A, Schmidt J, Vaccaro W, Conder M.J, Jenkins-West T, Levesque P. Benzopyran sulfonamides as $K_V1.5$ potassium channel blockers. *Bioorg Med Chem Lett.* 2007; 17:3271–3275. 10.1016/j.bmcl.2007.04.020.

15 Shen Z, Ramamoorthy PS, Hatzenbuhler NT, et al. Synthesis and structure–activity relationship of novel lactam-fused chroman derivatives having dual affinity at the 5-HT_{1A} receptor and the serotonin transporter. *Bioorg Med Chem Lett.* 2010;20: 222–227. https://doi.org/10.1016/j.bmcl.2009.10.134.

16 Afshar S, Shahidi S, Rohani AH, et al. Protective effects of 5-HT1A receptor antagonist and 5-HT2A receptor agonist on the biochemical and histological features in a rat model of Alzheimer's disease. *J Chem Neuroanat.* 2019;96:140–147. https://doi.org/10.1016/j.jchemneu.2019.01.008.

17 Jia CM, Zhang HX, Nie J, Ma JA. Catalytic Asymmetric Decarboxylative Mannich Reaction of Malonic Acid Half Esters with Cyclic Aldimines: Access to Chiral β-Amino Esters and Chroman-4-amines. *J Org Chem.* 2016;81:8561–8569. https://doi.org/10.1021/acs.joc.6b01750.

18 Passos GF, Medeiros R, Cheng D, et al. The Bradykinin B_1 Receptor Regulates Aβ Deposition and Neuroinflammation in Tg-SwDI Mice. *Amer J Path.* 2013;182: 1740–1749. https://doi.org/10.1016/j.ajpath.2013.01.021.

19 Viana H, Marques CS, Correia CA, et al. Novel Palladium-Catalyzed Intramolecular Addition of Aryl Bromides to Aldehydes as Key to the Synthesis of 3,3-Dimethyl-chroman-4-ones and 3,3-Dimethylchroman-4-ols. *Chem Select.* 2018;3:11333–11338. https://doi.org/10.1002/slct.201802889.

20 Talele TT. Natural-Products-Inspired Use of the *gem*-Dimethyl Group in Medicinal Chemistry. *J Med Chem.* 2018;61:2166–12110. https://doi.org/10.1021/acs.jmedchem.7b00315.

21 Otoguro K, Kuno F, Omura S. Arisugacins, selective acetylcholinesterase inhibitors of microbial origin. *Pharmacol Ther.* 1997;76:45–54. https://doi.org/10.1016/S0163-7258(97)00093-4.

22 Ramsay RR, Basile L, Maniquet A, et al. Parameters for Irreversible Inactivation of Monoamine Oxidase. *Molecules*. 2020;25(5908). https://doi.org/10.3390/molecules25245908.

23 Bacalhau, P., Mechanism of Action and Promising Treatments for Neurodegenerative Diseases, PhD thesis, University of Evora, 2018.

24 Claridge T.D.W. High-Resolution NMR Techniques in Organic Chemistry, 3rd Edition. Oxford, Elsevier; 2016.

25 (a) Totobenazara J, Bacalhau P, San Juan A, et al. Design, Synthesis and Bioassays of 3-Substituted-3-Hydroxyoxindoles for Cholinesterase Inhibition. *Chem Select.* 2016;1: 3580-3588. 10.1002/slct.201600932 (b) Bacalhau P, Fernandes L, Candeias F, et al. In silico, NMR and pharmacological evaluation of an hydroxyoxindole cholinesterase inhibitor. *Bioorg Med Chem.* 2019; 27:354-363. 10.1016/j.bmc.2018.12.007 (c) Bacalhau P, San Juan A.A, Goth A, et al. Insights into (S)-rivastigmine inhibition of butyrylcholinesterase (BuChE): Molecular docking and saturation transfer difference NMR (STD-NMR). *Bioorg. Chem.* 2016; 67:105-109. 10.1016/j.bioorg.2016.06.002.

26 Daina A, Michielin O, Zoete V. SwissADME: a free web tool to evaluate pharmacokinetics, drug-likeness and medicinal chemistry friendliness of small molecules. *Sci Rep.* 2017;7:42717. https://doi.org/10.1038/srep42717.

27 Lipinski A, Lombardo F, Dominy BW, et al. Experimental and computational approaches to estimate solubility and permeability in drug discovery and development settings. *Adv. Drug Del. Rev.* 2001;46:3–26. https://doi.org/10.1016/s0169-409x(00)00129-0.

28 Ali J, Camilleri P, Brown MB, et al. Revisiting the general solubility equation: in silico prediction of aqueous solubility incorporating the effect of topographical polar surface area. *J. Chem. Inf. Mod.* 2012;26:2950–2957. https://doi.org/10.1021/ci200387c.

29 Herter S, Medina F, Wagschal S, et al. Mapping the substrate scope of monoamine oxidase (MAO-N) as a synthetic tool for the enantioselective synthesis of chiral amines. *Bioorg. Med. Chem.* 2018;26:1338–1346. https://doi.org/10.1016/j.bmc.2017.07.023.

30 Ellman GL, Courtney KD, Andres Jr V, et al. new and rapid colorimetric determination of acetylcholinesterase activity. *Biochem Pharmacol.* 1961;7:88–95. https://doi.org/10.1016/0006-2952(61)90145-9.

31 Cornish-Bowden A. A simple graphical method for determining the inhibition constants of mixed, uncompetitive and non-competitive inhibitors. *Biochem J.* 1974; 137:143–144. https://doi.org/10.1042/bj1370143.

32 Affini A, Hagenow S, Zivkovic A, et al. Novel indanone derivatives as MAO-B/H_3R dual-targeting ligands for treatment of Parkinson's disease. *Eur J Med Chem.* 2018; 148:487. https://doi.org/10.1016/j.ejmech.2018.02.015.

33 Glide, Schrödinger, LLC, New York, NY; 2018.

34 Maestro, Schrödinger LLC, New York, NY, USA; 2018.

35 Berman HM, Westbrook J, Feng Z, et al. The Protein Data Bank. *Nucleic Acids Res.* 2000;28:235–242. https://doi.org/10.1093/nar/28.1.235.

36 Cheung J, Rudolph MJ, Burshteyn F, et al. Structures of Human Acetylcholinesterase in Complex with Pharmacologically Important Ligands. *J Med Chem.* 2012;55: 10282–10286. https://doi.org/10.1021/jm300871x.

37 Kosak U, Brus B, Knez D, et al. The Magic of Crystal Structure-Based Inhibitor Optimization: Development of a Butyrylcholinesterase Inhibitor with Picomolar Affinity and *in vivo* Activity. *J Med Chem.* 2018;61:119–139. https://doi.org/10.1021/acs.jmedchem.7b01086.

38 Reis J, Manzanella N, Cagide F, et al. Tight-Binding Inhibition of Human Monoamine Oxidase B by Chromone Analogs: A Kinetic, Crystallographic, and Biological Analysis. *J Med Chem.* 201; 61: 4203-4212. 10.1021/acs.jmedchem.8b00357.